Invariant template matching in systems with spatiotemporal coding: a matter of instability

Ivan Tyukin*, Tatiana Tyukina†, Cees van Leeuwen‡

December 3, 2008

Abstract

We consider the design principles of algorithms that match templates to images subject to spatiotemporal encoding. Both templates and images are encoded as temporal sequences of samplings from spatial patterns. Matching is required to be tolerant to various combinations of image perturbations. These include ones that can be modeled as parameterized uncertainties such as image blur, luminance, and, as special cases, invariant transformation groups such as translation and rotations, as well as un-modeled uncertainties (noise). For a system to deal with such perturbations in an efficient way, they are to be handled through a minimal number of channels and by simple adaptation mechanisms. These normative requirements can be met within the mathematical framework of weakly attracting sets. We discuss explicit implementation of this principle in neural systems and show that it naturally explains a range of phenomena in biological vision, such as mental rotation, visual search, and the presence of multiple time scales in adaptation. We illustrate our results with an application to a realistic pattern recognition problem.

*Laboratory for Perceptual Dynamics, RIKEN (Institute for Physical and Chemical Research) Brain Science Institute, 2-1, Hirosawa, Wako-shi, Saitama, 351-0198, Japan, e-mail: {tyukinivan}@brain.riken.jp; Department of Mathematics, University of Leicester, University Road, Licester, LE1 7RH, United Kingdom, e-mail: I.Tyukin@le.ac.uk

†Laboratory for Perceptual Dynamics, RIKEN (Institute for Physical and Chemical Research) Brain Science Institute, 2-1, Hirosawa, Wako-shi, Saitama, 351-0198, Japan, e-mail: {tatianat}@brain.riken.jp

‡**Corresponding author.** Laboratory for Perceptual Dynamics, RIKEN (Institute for Physical and Chemical Research) Brain Science Institute, 2-1, Hirosawa, Wako-shi, Saitama, 351-0198, Japan, e-mail: {ceesvl}@brain.riken.jp

Invariant template matching in systems with spatiotemporal coding: a matter of instability

Abstract

We consider the design principles of algorithms that match templates to images subject to spatiotemporal encoding. Both templates and images are encoded as temporal sequences of samplings from spatial patterns. Matching is required to be tolerant to various combinations of image perturbations. These include ones that can be modeled as parameterized uncertainties such as image blur, luminance, and, as special cases, invariant transformation groups such as translation and rotations, as well as un-modeled uncertainties (noise). For a system to deal with such perturbations in an efficient way, they are to be handled through a minimal number of channels and by simple adaptation mechanisms. These normative requirements can be met within the mathematical framework of weakly attracting sets. We discuss explicit implementation of this principle in neural systems and show that it naturally explains a range of phenomena in biological vision, such as mental rotation, visual search, and the presence of multiple time scales in adaptation. We illustrate our results with an application to a realistic pattern recognition problem.

1 Notational preliminaries

We define an image as a mapping $S_0(x, y)$ from a class of locally bounded mappings $\mathcal{S} \subseteq L_\infty(\Omega_x \times \Omega_y)$, where $\Omega_x \subseteq \mathbb{R}$, $\Omega_y \subseteq \mathbb{R}$, and $L_\infty(\Omega_x \times \Omega_y)$ is the space of all functions $f : \Omega_x \times \Omega_y \to \mathbb{R}$ such that $\|f\|_\infty = \operatorname{ess\,sup}\{\|f(x, y)\|, x \in \Omega_x,\ y \in \Omega_y\} < \infty$. Symbols x, y denote variables on different spatial axes. The value of $S_0(x, y)$ depends on the domain of interest (e.g. brightness, contrast, color, etc.). Our interpretation of images as functions from $L_\infty(\Omega_x \times \Omega_y)$ is motivated mostly by the fact that in the domain of vision the characteristic values are usually bounded. We will treat them as such unless information to the contrary is available.

We assume that within a system an image is represented as a set of pre-specified templates, $S_i(x, y) \in \mathcal{S}$, $i \in \mathcal{I} \subset \mathbb{N}$, where $\mathcal{I}$ is the set of indices of all templates associated with the image $S_0(x, y) \in \mathcal{S}$. Symbol $\mathcal{I}^+$ is reserved for $\mathcal{I}^+ = \mathcal{I} \cup 0$.

The solution of a system of differential equations $\dot{\mathbf{x}} = \mathbf{f}(\mathbf{x}, t, \boldsymbol{\theta}, \mathbf{u}(t))$, $\mathbf{u} : \mathbb{R}_{\geq 0} \to \mathbb{R}^m$, $\boldsymbol{\theta} \in \mathbb{R}^d$ passing through point $\mathbf{x}_0$ at $t = t_0$ will be denoted for $t \geq t_0$ as $\mathbf{x}(t, \mathbf{x}_0, t_0, \boldsymbol{\theta}, \mathbf{u})$, or simply as $\mathbf{x}(t)$ if it is clear from the context what the values of $\mathbf{x}_0, \boldsymbol{\theta}$ are and how the function $\mathbf{u}(t)$ is defined.

By $L^n_\infty[t_0, T]$, $t_0 \geq 0$, $T \geq t_0$ we denote the space of all functions $\mathbf{f} : \mathbb{R}_{\geq 0} \to \mathbb{R}^n$ such that $\|\mathbf{f}\|_{\infty,[t_0,T]} = \operatorname{ess\,sup}\{\|\mathbf{f}(t)\|, t \in [t_0, T]\} < \infty$; $\|\mathbf{f}\|_{\infty,[t_0,T]}$ stands for the $L^n_\infty[t_0, T]$ norm of $\mathbf{f}(t)$.

Let $\mathcal{A}$ be a set in $\mathbb{R}^n$ and $\|\cdot\|$ be the usual Euclidean norm in $\mathbb{R}^n$. By the symbol $\|\cdot\|_{\mathcal{A}}$ we denote the following induced norm:

$$\|\mathbf{x}\|_{\mathcal{A}} = \inf_{\mathbf{q}\in\mathcal{A}}\{\|\mathbf{x}-\mathbf{q}\|\}$$

In case x is a scalar and $\Delta \in \mathbb{R}_{>0}$, notation $\|x\|_{\Delta}$ stands for the following

$$\|x\|_{\Delta} = \begin{cases} |x|-\Delta, & |x|>\Delta \\ 0, & |x|\leq\Delta \end{cases}$$

2 Introduction

This article deals with the challenges and opportunities that spatiotemporal representation of visual information offers for visual pattern recognition. We will consider spatiotemporal pattern representation in the framework of template matching, the oldest and most common method for detecting an object in an image. According to this method the image is searched for items that match a template. A template consists of one or more local arrays of values representing the object, e.g. intensity, color, or texture. A similarity value[1] is calculated between these templates and domains of the image, and a domain is associated with the template once their similarity exceeds a given threshold.

Despite the simple and straightforward character of this method, its implementation requires us to consider two fundamental problems. The first relates to *what* features should be compared between the image $S_0(x,y)$ and the template $S_i(x,y)$, $i \in \mathcal{I}$. The second problem is *how* this comparison should be done.

The normative answer to the question of *what* features should be compared invokes solving the issue of optimal image representation, ensuring most effective utilization of available resources and, at the same time, minimal vulnerability to uncertainties. Principled solutions to this problem are well-known from the literature and can be characterized as *spatial sampling*. For example, when the resource is frequency bandwidth of a single measurement mechanism, the optimality of spatially sampled representations is proven in Gabor's seminal work (Gabor, 1946)[2]. In classification problems, the advantage of spatially sampled image representations is demonstrated in (Ullman et al., 2002). In general, these representations are

[1] Traditionally a correlation measure is commonly used for this purpose (Jain et al., 2000).

[2] Consider, for instance, a system which measures image $S_i(x,y)$ using a set of sensors $\{m_1,\ldots,m_n\}$. Each sensor m_i is capable of measuring signals within the given frequency band Δ_i at the location x_i in corresponding spatial dimension x. Then according to (Gabor, 1946), sensor m_i can measure both the frequency content of a signal and its spatial location with minimal uncertainty only if the signal has a Gaussian envelope in x: $S_i(x,y) \sim e^{\sigma_i^{-2}(x-x_i)^2}$. In other words, the signal should be practically spatially bounded. This implies that the image must be spatially sampled.

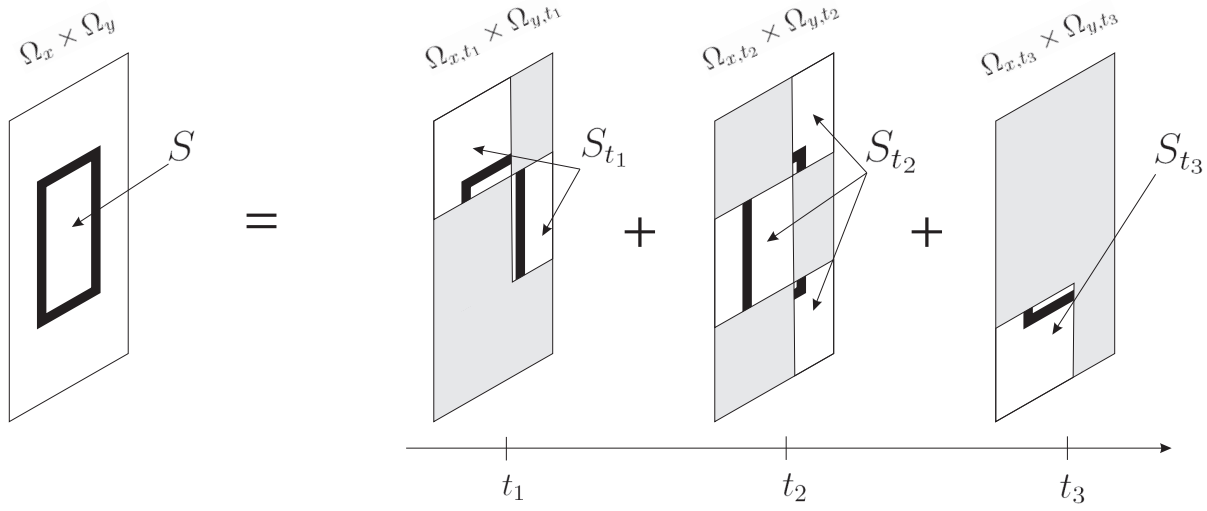

Figure 1: Spatial sampling of image $S(x, y) : \Omega_x \times \Omega_y \rightarrow \mathbb{R}_+$ according to the factorization of $\Omega_x \times \Omega_y$ into subsets $\Omega_{x,t_1} \times \Omega_{y,t_1}$, $\Omega_{x,t_2} \times \Omega_{y,t_2}$, $\Omega_{x,t_3} \times \Omega_{y,t_3}$

obtained naturally when balancing the system resources and uncertainties in the measured signal. A simple argument supporting this claim is provided in Appendix 1.

A variety of sophisticated spatial sampling methods exists (Gabor, 1946; Blake et al., 1994; Bueso et al., 1999; Lee & Yuille, 2006). Here we limit ourselves to spatial sampling in its elementary form, which is achieved by factorizing both the domain $\Omega_x \times \Omega_y$ of the image S_0 and the templates S_i, $i \in \mathcal{I}$ into subsets:

$$\Omega_x \times \Omega_y = \bigcup_t \Omega_{x,t} \times \Omega_{y,t},\ t \in \Omega_t,\ \Omega_{x,t} \subseteq \Omega_x,\ \Omega_{y,t} \subseteq \Omega_y. \tag{1}$$

Factorization (1) induces sequences $\{S_{i,t}\}$, where $S_{i,t}$ are the restrictions of mappings S_i to the domains $\Omega_{x,t} \times \Omega_{y,t}$. These sequences constitute sampled representations of S_i, $i \in \mathcal{I}^+$ (see Figure 1). Notice that the sampled image and template representations $\{S_{i,t}\}$ are, strictly speaking, sequences of functions. In order to compare them, scalar values $f(S_{i,t})$ are normally assigned to each $S_{i,t}$. Examples include various functional norms, correlation functions, spectral characterizations (average frequency or phase), or simply weighted sums of the values of $S_{i,t}$ over the entire domain $\Omega_{x,t} \times \Omega_{y,t}$. Formally, f could be defined as a functional, which maps restrictions $S_{i,t}$ into the field of real numbers:

$$f : L_\infty(\Omega_{x,t} \times \Omega_{y,t}) \rightarrow \mathbb{R} \tag{2}$$

This formulation allows a simple representation of images and templates as sequences of scalar values $\{f(S_{i,t})\}$, $i \in \mathcal{I}^+$, $t \in \Omega_t$. We will therefore adopt this method here.

The answer to the second question, *how* the comparison is done, involves finding the best and simplest way possible to utilize the information that a given image representation provides, while at the same time ensuring invariance to basic distortions. Even though considerable attention has been given to this problem, a unified solution is not yet available. The primary goal of our current contribution is to present a unified framework to solve this problem for a class of systems of sufficiently broad theoretical and practical relevance.

We consider the class of systems in which spatially sampled image representations are encoded as temporal sequences. In other words, parameter t in the notation $f(S_{i,t})$ is the time variable. This type of representation is frequently encountered in neuronal networks (Gutig & Sompolinsky, 2006) (see also references therein). Examples of similar representation schemes are widely reported in the neuroscience literature. For example (Alonso et al., 1996) show that patches of visual stimuli which are perceived as spatially close by the processing system (e.g. when the receptive fields of individual cells overlap) are encoded by similar firing spike patterns and vice versa. In our model spatially non-overlapping patches are represented by different sequences $\{f(S_{i,t})\}$, and identical images have identical temporal representations. Hence such systems have a claim to biological plausibility. In addition, they enable a simple solution to a well-known dilemma. This is about whether comparison between templates and image domains should be made on a large, i.e. global, or on a small, i.e. local scale. The solution to this dilemma consists in temporal integration. Let, for instance, $\Omega_t = [0, T]$, $T \in \mathbb{R}_{>0}$. Then an example of a temporally-integral, yet spatially sampled, representation is:

$$f(S_{i,t}) \mapsto \phi_i(t) = \int_0^t f(S_{i,\tau}) d\tau,\ t \in [0, T],\ i \in \mathcal{I}^+ \tag{3}$$

The temporal integral $\phi_i(t)$ contains both spatially local and global image characterizations. Whereas its time-derivative at t equals to $f(S_{i,t})$ and corresponds to spatially sampled, local representation $S_{i,t}$, the global representation $\phi_i(T)$ equals to the integral, cumulative characterization of S_i. An example illustrating these properties is provided in Figure 2. A further advantage of spatiotemporal representations $\phi_i(t)$ is that they offer powerful mechanisms for comparison, processing and matching of $\phi_i(t)$, $i \in \mathcal{I}$. These mechanisms can generally be characterized in terms of dynamic oscillator networks which synchronize when their inputs are converging to the same function.

Despite advantages such as optimality, simplicity and biological plausibility, there are theoretical issues which have prevented wide application of spatiotemporal representations to template matching. The most important issues, from our point of view, are, first, how to achieve effective recognition in the presence of modeled disturbances, of which the most

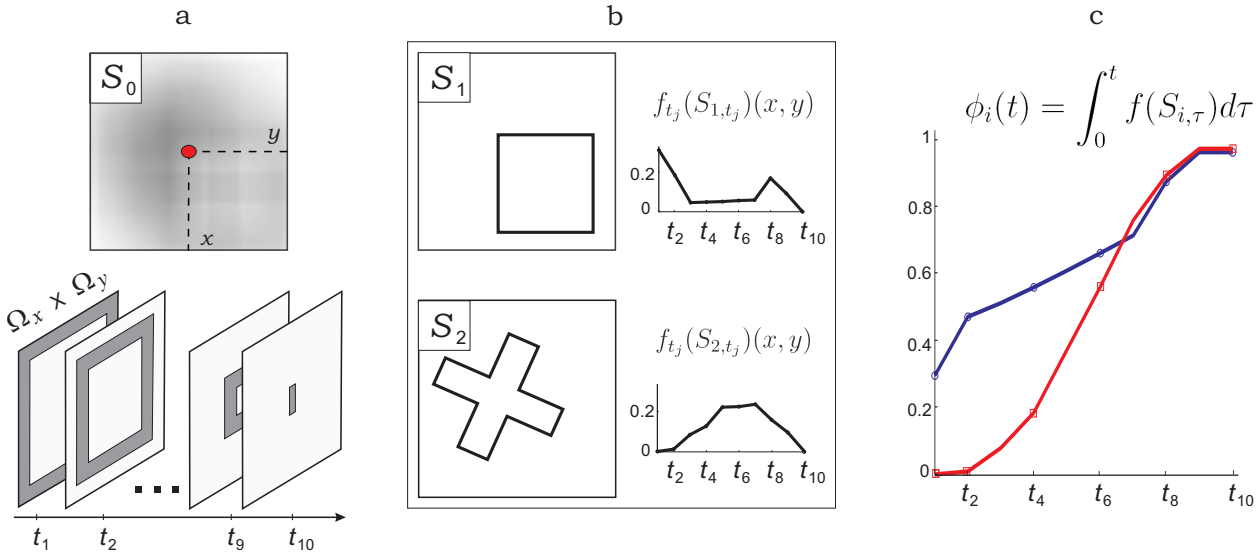

Figure 2: Spatiotemporal image representation via spatial sampling and temporal integration. Panel a contains the original object, S_0; (x, y) marks a point on the image with respect to which the correlation is calculated; factorization of the domain $\Omega_x \times \Omega_y$ into ten arbitrary, here chosen to be nonintersecting, subsets $\Omega_x \times \Omega_y = \cup_{j=1}^{10} \Omega_{x,t_j} \times \Omega_{y,t_j}$. Panel b – templates S_1, S_2 and plots of $f_{t_j}(S_{1,t_j})(x, y)$, $f_{t_j}(S_{2,t_j})(x, y)$ – the values of the normalized correlation between $S_{i,t_j} = S_i(\Omega_{x,t_j} \times \Omega_{y,t_j})$ and $S_0(\Omega_{x,t_j} \times \Omega_{y,t_j})$. Panel c – plots of the values of (3) as a function of parameter t for templates S_1 (blue line) and S_2 (red line).

common ones are blur, luminance, and rotational and translational distortions. Second, how to take into account inevitable unmodeled perturbations.

The first class of problems amounts to finding a possible transformation of the template that can model the disturbance. Similarly to the framework of deformable templates (Amit, 2002; Amit, Grenader, & Piccioni, 1991) we assume a disturbance model to be a mapping which maps the template, S_i, into the image, S_0. Unlike in traditional deformable templates approaches (Miller & Younes, 2001) we do not wish to assume, however, that this mapping is invertible or forms a group action. This is because we would like to enable multiple solutions to the matching problem, as is appropriate in case of biological vision. Furthermore, even when a transformation is invertible the inverse operation could be highly susceptible to small image noise which, for instance, is the case for integration/differentiation operations. Finally, for the sake of computational effectiveness we would like to refrain from posing the matching problem as an optimization problem in the space of functions (transformations).

For these reasons we will consider modeled disturbances as known, yet *nonlinearly parameterized mappings*. Parameters of these mappings, however, are allowed to be uncertain. This enables us to consider non-invertible and generally nonlinear image transformations

such as blur. Standard group actions, such as rotation, translation, or scaling can be treated as special cases of such transformations. Finding a suitable transformation of the template amounts to designing a *dynamic* identification/adaptation algorithm with proven efficiency in reconstructing parameters of generally nonlinear perturbations. The latter is an optimization problem in finite (low) dimensional space as compared to optimization in the infinite-dimensional space of functions. Currently available approaches to designing such algorithms either are restricted to linear parametrization of disturbances, involve overparametrization, or use domination feedback. Yet, linear parametrization is too restricted to be plausible, overparametrization is expensive in terms of the number of adjustable units, and domination lacks adequate sensitivity. For these reasons current methods remain unsatisfactory. We will, therefore, propose a novel solution to these problems.

The second class of problems, recognition in presence of unmodeled perturbations, calls for procedures for recognizing an image from its perturbed temporal representation $\phi_i(t)$. At this level the system is facing the contradictory requirements of ensuring robust performance while being highly sensitive to minor changes in the stimulation. Here, too, we will advocate a solution.

The proposed solution to both types of problem diverges from current approaches, which invoke the concept of Lyapunov-stable attractors. We concur that by allowing the system to converge on an attractor, these methods are able to eliminate modeled and unmodeled distortions and thus, for instance, complete an incomplete pattern in the input (Amit et al., 1985; Fuchs & Haken, 1988; Herz et al., 1989; Hopfield, 1982; Ritter & Kohonen, 1989). The strength of these systems resides in the robustness inherent in uniform asymptotic Lyapunov stability. There is, however, a corresponding weakness: such systems are generally lacking in flexibility. Each stable attractor in the system represents one pattern; but often an image contains more than one pattern. When the system is steered to one template, the other is lost from the representation. It would, therefore, be preferable to have a system that allows flexible switching between alternative patterns and exploration of alternatives beyond the ones currently recognized. Yet, the very notion of stable convergence to an attractor provides an obstacle to switching and exploration. Furthermore, as we will show, for a class of the images with multiple representations and various symmetries, globally stable solutions to the problem of invariant template matching may not even exist.

We propose a unifying framework capable of combining robustness and flexibility. In contrast to common intuitions, which aim at achieving desired robustness by means of stable attractors, we advocate instability as an advantageous substitute. More precisely, we

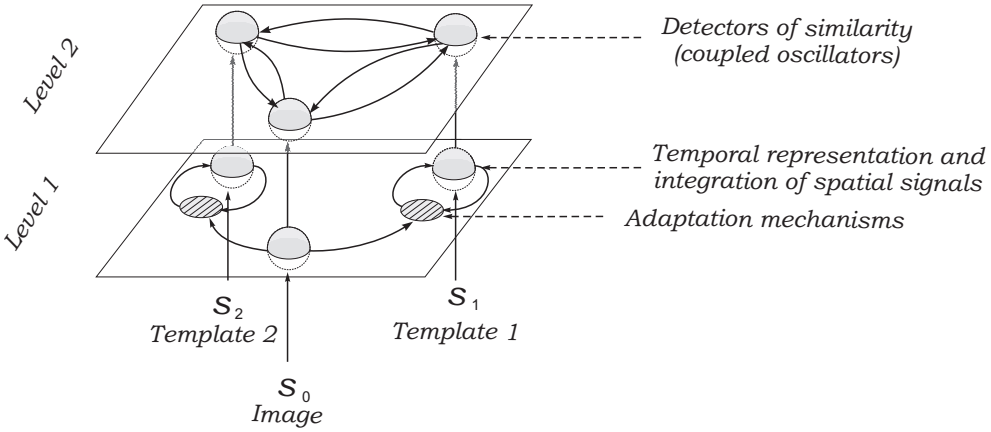

Figure 3: General scheme of a system for adaptive template matching using temporal codes. Level 1 contains the adaptive compartments. Its functional role is to ensure invariance to modeled uncertainties. Level 2 corresponds to the comparison compartments and consists of coupled nonlinear oscillators. Solid arrows represent the information flow in the system.

consider a specific type of instability inherent to solutions converging to proper weakly attracting sets and Milnor attractors (Milnor, 1985). The utility of weakly attracting sets has already been acknowledged in the general context of modeling brain activity and decision-making. For example, in networks of nonlinear oscillators and coupled maps emergence of Milnor attractors is considered as a precursor of chaotic itinerancy – the systems's dynamic state corresponding to sporadic chaotic switching of trajectories from one quasi-attractor (ghost attractor) to another (Tsuda & Fujii, 2007) [3]. Here we demonstrate that the concept of weakly attracting sets provides a unifying framework for solving pattern recognition problems. We show that trading the habitual requirement of Lyapunov stability for a more relaxed property of convergence to weakly attracting sets provides both the necessary invariance and the flexibility needed for invariant template matching. Doing so, furthermore, allows us to overcome challenging technical issues related to nonlinearity and non-convexity of modeled uncertainties in tuning of parameters for spatio-temporal encoding. Finally, the relevance of Milnor attractors has been argued extensively for models of information processing in the human brain (see (van Leeuwen, 2008) for review). We will briefly illustrate with examples how Milnor attractors could instill functionality in the brain.

To illustrate these principles we designed a recognition system consisting of two major components (see Figure 3). The first is an adaptive component in which information is processed by a class of spatiotemporal filters. These filters represent internal models of distortions. The models of most common distortions, including rotation, translation, and blur,

[3]See also related concepts of heteroclinic channels (Rabinovic et al., 2008) and relaxation times (Gorban, 2004)

are often nonlinearly parameterized. Until recently, adequate compensatory mechanisms for nonlinearly parameterized uncertainties have been unexplored territory. In recent work (Tyukin & van Leeuwen, 2005) we have shown that the problem of nonlinear parameterization could, in principle, be solved within the concept of Milnor or weak, unstable attractors. Here we provide a solution to this problem that will enable systems to deal with specific nonlinearly parameterized models of distortions that are typical for a variety of optical and geometrical perturbations.

The second major component of our system consists of a network of coupled nonlinear oscillators. These operate as coincidence detectors. Each oscillator in our system represents a Hindmarsh-Rose model neuron. These model neurons are generally believed to provide a good qualitative approximation to biological neuron behavior. At the same time they are computationally cost-effective (Izhikevich, 2004). For networks of these oscillators we prove, first of all, boundedness of the state of the perturbed solutions. In addition, we specify the parameter values which lead to emergence of globally stable invariant manifolds in the system state space. Although we do not provide explicit criteria for the meta-stability that quasi-attractors provide in this class of networks, the conditions presented allow us to narrow substantially the domain of relevant parameter values in which this behavior is to be found.

There is an interesting consequence to the unstable character of the compensation for modeled perturbations. When the system negotiates multiple classes of uncertainties simultaneously (e.g. focal/contrast and intensity/luminance), different types of compensatory adjustments are made at different time scales. Adaptation at different time scales is a well-known phenomenon in biological visual systems (Baccus & Meister, 2002; Demontis & Cervetto, 2002; Sharpe & Stockman, 1999; Smirnakis et al., 1997), in particular when light/dark adaptation is combined with optical/neuronal blur (Hofer & Williams, 2002; Mather, 2006; Mon-Williams et al., 1998; Rodieck, 1998). Our analytical study suggests that this difference in time-scales emerges naturally as a sufficient condition for the proper operation of our system.

This paper is organized as follows. In Section 3 we provide a formal description of the class of images and templates, and formally state the problems of our study. In Section 4 we provide the main results of our present contribution. In Section 5 we discuss the theoretical results and relate them to relevant observations in the empirical literature on visual perception and adaptation. In Section 6 we provide an illustrative example of a simple system ensuring invariant recognition of rotated and shifted templates in images with varying intensity. We also present an application of our approach to a realistic pattern

recognition problem: the detection of morphological changes in dendritic spines based on measurements obtained from a multiphoton scanning microscope. Section 7 concludes the paper.

3 Preliminaries and problem formulation

We assume that the values $S_0(x, y)$ of the original image are not available explicitly to the system; it only is able to measure perturbed values of $S_0(x, y)$. Perturbation is defined as a mapping $\mathcal{F}$:

$$\mathcal{F}[S_0, \boldsymbol{\theta}] : \; L_\infty(\Omega_x \times \Omega_y) \times \mathbb{R}^d \to L_\infty(\Omega_x \times \Omega_y),$$

where $\boldsymbol{\theta}$ is the vector of parameters of the perturbation. The values of $\boldsymbol{\theta}$ are assumed to be unknown a-priori, whereas the mapping $\mathcal{F}$ is known.

In systems for processing spatial information, mappings $\mathcal{F}$ often belong to a specific class that can be defined as follows:

$$\begin{aligned} \mathcal{F}[S_0, \boldsymbol{\theta}] &= \theta_1 \cdot \bar{\mathcal{F}}[S_0, \theta_2], \;\; \theta_1 \in \mathbb{R}, \;\; \theta_2 \in \mathbb{R} \\ \bar{\mathcal{F}}[S_0, \theta_2] &: L_\infty(\Omega_x \times \Omega_y) \times \mathbb{R} \to L_\infty(\Omega_x \times \Omega_y), \\ \boldsymbol{\theta} &= (\theta_1, \theta_2) \end{aligned} \tag{4}$$

Parameter $\theta_1 \in [\theta_{1,\min}, \theta_{1,\max}] \subset \mathbb{R}$ in (4) models *linear* perturbations, for instance variations of overall brightness or intensity of the original image S_0. The parameter can also be interpreted as an a-priori unknown gain in the measurement channel of a sensor. Mapping $\bar{\mathcal{F}}(S_0, \theta_2)$ in (4), parameterized by $\theta_2 \in [\theta_{2,\min}, \theta_{2,\max}] \subset \mathbb{R}$, corresponds to typical *nonlinear* perturbations of image S_0. Table 1 provides examples of such perturbations, their mathematical models and the physical meaning of parameter θ_2. Throughout the paper we assume that mappings $\bar{\mathcal{F}}[S_0, \theta_2]$ are Lipschitz in θ_2:

$$\begin{aligned} \exists \; D \in \mathbb{R}_{>0} : \quad & \left|\bar{\mathcal{F}}[S_0, \theta_2'](x, y) - \bar{\mathcal{F}}[S_0, \theta_2''](x, y)\right| \leq D|\theta_2' - \theta_2''|, \\ & \forall \; (x, y) \in \Omega_x \times \Omega_y, \; \theta_2', \theta_2'' \in \mathbb{R} \end{aligned} \tag{5}$$

Notice that, strictly speaking, several typical transformations such as translation, scaling, and rotation, are not always Lipschitz. This is because image S_0 can, for instance, have sharp edges which corresponds to discontinuities in x, y. In practice, however, prior application of a blurring linear filter will render sharp edges in an image smooth, thus assuring that condition (5) applies[4].

[4]In biological vision discontinuity of S_0 in x, y corresponds to images with abrupt local changes in brightness along spatial dimensions x, y. Although this is a rather common situation in nature, in visual systems actual images S_0 rarely reach a sensor in their spatially discontinuous form. In fact, prior to reaching the sensory receptors, they are subject to optical linear filtering. Therefore images that reach the sensor are always smooth. Hence condition (5) will generally be satisfied.

Table 1: Examples of typical nonlinear perturbations of S_0. Parameter Δ_θ in the right column is a positive constant

Physical meaning	Mathematical model of $\bar{\mathcal{F}}[S_0, \theta_2]$	Domain of physical relevance
Translation (in x dimension) θ_2 – shift	$\bar{\mathcal{F}}[S_0, \theta_2] = S_0(x + \theta_2, y)$	$-\Delta_\theta \leq \theta_2 \leq \Delta_\theta$
Scaling (in x dimension) θ_2 – scaling factor	$\bar{\mathcal{F}}[S_0, \theta_2] = S_0(\theta_2 \cdot x, y)$	$0 < \theta_2 \leq \Delta_\theta$
Rotation around the origin θ_2 – angle of rotation	$\bar{\mathcal{F}}[S_0, \theta_2] = S_0(x_r(x, y, \theta_2), y_r(x, y, \theta_2))$ $x_r(x, y, \theta_2) = \cos(\theta_2)x - \sin(\theta_2)y$ $y_r(x, y, \theta_2) = \sin(\theta_2)x + \cos(\theta_2)y$	$0 \leq \theta_2 \leq 2\pi$
Image blur (not normalized) (Banham & Katsaggelos, 1997) θ_2 – blur parameter	$\bar{\mathcal{F}}[S_0, \theta_2] = \int_{\Omega_x \times \Omega_y} h \cdot S_2(\xi, \gamma) d\xi d\gamma$ 1) Gaussian: $h = \exp^{-\frac{1}{\theta_2}((x-\xi)^2 + (y-\gamma)^2)}$ 2) Out-of-focus: $h = \begin{cases} \frac{1}{\pi\theta_2^2}, & \sqrt{(x-\xi)^2 + (y-\gamma)^2} \leq \theta_2 \\ 0, & \text{else} \end{cases}$	$0 < \theta_2 \leq \Delta_\theta$

The image $\mathcal{F}[S_0, \boldsymbol{\theta}]$ is assumed to be spatially sampled according to factorization (1):

$$\mathcal{F}_t[S_0, \boldsymbol{\theta}](x, y) = \begin{cases} \mathcal{F}[S_0, \boldsymbol{\theta}](x, y), & (x, y) \in \Omega_{x,t} \times \Omega_{y,t}, \\ 0, & \text{else} \end{cases} \qquad t \in \Omega_t \tag{6}$$

Because index t in (6) is assumed to be a time variable we let $\Omega_t = [0, \infty)$. To each $\mathcal{F}_t[S_0, \boldsymbol{\theta}]$ a value $f(\mathcal{F}_t[S_0, \boldsymbol{\theta}]) \in \mathbb{R}$ is assigned. Formally this procedure can be defined by a functional which maps mappings $\mathcal{F}_t[S_0, \boldsymbol{\theta}]$ into the real values:

$$f : L_\infty(\Omega_x \times \Omega_y) \to \mathbb{R}. \tag{7}$$

In the singular case, when $\Omega_{x,t} \times \Omega_{y,t}$ is a point (x_t, y_t), the mapping $\mathcal{F}_t[S_0, \boldsymbol{\theta}](x, y)$ and functional f will be defined as $f = \mathcal{F}_t[S_0, \boldsymbol{\theta}](x_t, y_t) = \mathcal{F}[S_0, \boldsymbol{\theta}](x_t, y_t)$.

We concentrated our efforts on obtaining a principled solution to the problem of invariant template matching in systems with spatiotemporal processing of information. For this reason

Table 2: Examples of spatially-sampled representations of S_0

Physical meaning	Mathematical model of f
Spectral power within the given frequency bands: $\omega_x \in [\omega_a, \omega_b]$, $\omega_y \in [\omega_c, \omega_d]$	$f = \int_{\omega_a}^{\omega_b} \int_{\omega_c}^{\omega_d} \left\| \int_{\Omega_x \times \Omega_y} \mathcal{F}_t[S_0, \boldsymbol{\theta}](x,y) e^{-j(\omega_x x + \omega_y y)} dx dy \right\| d\omega_x d\omega_y$
Weighted sum (for instance, convolution with exponential kernel)	$f = \int_{\Omega_x \times \Omega_y} \mathcal{F}_t[S_0, \boldsymbol{\theta}](x,y) e^{-\lvert x-x_0\rvert - \lvert y-y_0\rvert} dx dy$ (x_0, y_0) is the reference, "attention" point
Scanning the image along a given trajectory $(x(t), y(t)) = (\xi(t), \gamma(t))$	$\Omega_{x,t} \times \Omega_{y,t} = (\xi(t), \gamma(t))$ $f = \mathcal{F}[S_0, \boldsymbol{\theta}](\xi(t), \gamma(t))$

we prefer not to provide a specific description of functionals f. We do, however, restrict our consideration to functionals that are both *linear* and Lipschitz, i.e. ones satisfying the following constraints:

$$f(\kappa\mathcal{F}) = \kappa f(\mathcal{F}),\ \forall\ \kappa \in \mathbb{R},\quad |f(\mathcal{F}) - f(\mathcal{F}')| \le D_2 \|\mathcal{F} - \mathcal{F}'\|_\infty,\quad D_2 \in \mathbb{R}_{>0} \tag{8}$$

Examples of functionals f satisfying conditions (8) and their physical interpretations are provided in Table 2.

Taking into account (4), (6) and the fact that f is linear, the following equality holds

$$f(\mathcal{F}_t[S_0, \boldsymbol{\theta}]) = \theta_1 f(\bar{\mathcal{F}}_t[S_0, \theta_2]),\quad \bar{\mathcal{F}}_t[S_0, \theta_2] = \begin{cases} \bar{\mathcal{F}}[S_0, \theta_2](x,y), & (x,y) \in \Omega_{x,t} \times \Omega_{y,t}, \\ 0, & \text{else} \end{cases} \tag{9}$$

For the sake of compactness, in what follows we replace $f(\bar{\mathcal{F}}_t[S_0, \theta_2])$ in the definition of $f(\mathcal{F}_t[S_0, \boldsymbol{\theta}])$ in (9) with the following notation:

$$f(\bar{\mathcal{F}}_t[S_0, \theta_2]) = f_0(t, \theta_2),\ \ f_0 : \Omega_t \times \mathbb{R} \to \mathbb{R} \tag{10}$$

Notation $f_0(t, \theta_2)$ in (10) allows us to emphasize the dependence of f on unknown θ_2, time variable t, and original image S_0. Subscript "0" in (10) indicates that $f_0(t, \theta_2)$ corresponds to the sampled and perturbed S_0 (equations (4), (7), (8)), and argument θ_2 is the nonlinear parameter of the perturbation applied to the image. Adhering to this logic, we introduce

the notation

$$f(\mathcal{F}_t[S_i, \boldsymbol{\theta}]) = \theta_1 f(\bar{\mathcal{F}}_t[S_i, \theta_2]) = \theta_1 f_i(t, \theta_2),$$

where subscript "i" indicates that $f_i(t, \theta_2)$ corresponds to the perturbed and sampled template S_i, and θ_2 is the nonlinear parameter of the perturbation applied to the template.

Let us now specify the class of schemes realizing temporal integration of spatially sampled image representations. Explicit realization of temporal integration (3) is not feasible because it may lead to unbounded outputs for a wide class of relevant signals, for instance signals that are constant or periodic with a nonzero average. The behavior of a temporal integrator (3), however, can be fairly well approximated by a first-order linear filter. For the sampled image and template representations $\theta_1 f_i(t, \theta_2)$, these filters can be defined as follows:

$$\begin{aligned} \dot{\phi}_0 &= -\frac{1}{\tau}\phi_0 + k \cdot \theta_1 f_0(t, \theta_2) \\ \dot{\phi}_i &= -\frac{1}{\tau}\phi_i + k \cdot \theta_1 f_i(t, \theta_2),\ k, \tau \in \mathbb{R}_{>0},\ i \in \mathcal{I} \end{aligned} \tag{11}$$

In contrast to (3), for filters (11) it is ensured that their state remains bounded for bounded inputs. In addition, on a first approximation, equations (11) present a simple model of neural sensors, collecting and encoding spatially-distributed information in the form of a function of time[5]. With respect to the physical realizability of (11), in addition to requirements (5), (8) we shall only assume that spatially sampled representations $\theta_1 f_i(t, \theta_2)$, $i \in \mathcal{I}^+$ of S_i ensure the existence of solutions for system (11).

Consider the dynamics of variables $\phi_0(t)$ and $\phi_i(t)$, $i \in \mathcal{I}$ defined by (11). We say that the i-th template matches the image iff for some given $\varepsilon \in \mathbb{R}_{\geq 0}$ the following condition holds

$$\limsup_{t \to \infty} |\phi_0(t) - \phi_i(t)| \leq \varepsilon. \tag{12}$$

The problem, however, is that parameters θ_1, θ_2 in (11) are unknown a-priori. While perturbations affect the image directly, they do not necessarily influence the templates. Rather to the contrary, for consistent recognition the templates are better kept isolated from external perturbations – at least within the time frame of pattern recognition, although they may, of course, be affected by adaptive learning on a larger time scale. Having fixed, unmodified templates in comparison with perturbed image representations implies that even in the cases when objects corresponding to the templates are present in the image, temporal image

[5]In principle, equation (11) can be replaced with a more plausible model of temporal integration such as integrate-and-fire, Fitzhugh-Nagumo, or Hodgkin-Huxley model neurons. These extensions, however, are not immediately relevant for the purpose of our current study. We decided to keep the mathematical description of the system as simple as possible, keeping in mind the possibility of extension to a wider class of temporal integrators (11).

representation $\phi_0(t)$ will likely be different from any of the templates, $\phi_i(t)$. This will render the chances that condition (12) is satisfied very small, so a template would almost never be detected in an image.

We propose that the proper way for a system to meet requirement (12) is to mimic the effect of disturbances in the template. In order to achieve this, the template matching system should be able to track the unknown values of parameters θ_1, θ_2. Hence the original equations for temporal integration (11) will be replaced with the following:

$$\begin{aligned} \dot{\phi}_0 &= -\frac{1}{\tau}\phi_0 + k \cdot \theta_1 f_0(t, \theta_2) \\ \dot{\phi}_i &= -\frac{1}{\tau}\phi_i + k \cdot \hat{\theta}_{i,1} f_i(t, \hat{\theta}_{i,2}),\ k, \tau \in \mathbb{R}_{>0},\ i \in \mathcal{I} \end{aligned} \tag{13}$$

where $\hat{\theta}_{i,1}$, $\hat{\theta}_{i,2}$ are the estimates of θ_1, θ_2. The estimates $\hat{\theta}_{i,1}$, $\hat{\theta}_{i,2}$ must track instantaneous changes of θ_1, θ_2. The information required for such an estimation should be kept at a minimum. An acceptable solution would be a simple mechanism capable of tracking the perturbations from the measurements of the image alone. The formal statement of this problem is provided below:

Problem 1 (Invariance) *For a given image S_0, template S_i, and their spatiotemporal representations satisfying (5), (8), and (13), find estimates*

$$\hat{\theta}_{i,1} = \hat{\theta}_{i,1}(t, \tau, \kappa, \phi_0, \phi_i), \quad \hat{\theta}_{i,2} = \hat{\theta}_{i,2}(t, \tau, \kappa, \phi_0, \phi_i) \tag{14}$$

as functions of time t, variables ϕ_0, ϕ_i and parameters τ, κ such that for all possible values of parameters $\theta_1 \in [\theta_{1,\min}, \theta_{1,\max}]$, $\theta_2 \in [\theta_{2,\min}, \theta_{2,\max}]$

1) solutions of system (13) are bounded;

2) in case $f_0 = f_i$ property (12) is ensured, and

3) the following holds for some $\theta_1' \in [\theta_{1,\min}, \theta_{1,\max}]$, $\theta_2' \in [\theta_{2,\min}, \theta_{2,\max}]$:

$$\begin{aligned} \limsup_{t\to\infty} |\hat{\theta}_{i,1}(t, \tau, \kappa, \phi_0(t), \phi_i(t)) - \theta_{i,1}'| \le \varepsilon_{\theta,1},\ \varepsilon_{\theta,1} \in \mathbb{R}_+ \\ \limsup_{t\to\infty} |\hat{\theta}_{i,2}(t, \tau, \kappa, \phi_0(t), \phi_i(t)) - \theta_{i,2}'| \le \varepsilon_{\theta,2},\ \varepsilon_{\theta,2} \in \mathbb{R}_+ \end{aligned} \tag{15}$$

Once the solution to Problem 1 is found, the next step will be to ensure that similarities (12) are registered in the system. In line with Figure 3, we propose that detection of similarities is realized by a system of coupled oscillators. In particular, we require that states of oscillators i and 0 converge as soon as the signals $\phi_0(t)$, $\phi_i(t)$ become sufficiently close.

In the present article we restrict ourselves to the class of systems composed of linearly coupled Hindmarsh-Rose model neurons (Hindmarsh & Rose, 1984). This choice is motivated

by the fact that these oscillators can reproduce a broad class of behaviors observed in real neurons while being computationally efficient (Izhikevich, 2004). A network of these neural oscillators can be mathematically described as follows:

$$\mathcal{S}_{D_i}: \begin{cases} \dot{x}_i &= -ax_i^3 + bx_i^2 + y_i - z_i + I + u_i + \phi_i(t), \\ \dot{y}_i &= c - dx_i^2 - y_i, \\ \dot{z}_i &= \epsilon(s(x_i + x_0) - z_i), \end{cases} \quad i \in \mathcal{I}^+ \tag{16}$$

Variables x_i, y_i, z_i correspond to membrane potential, and aggregated fast and slow adaptation currents, respectively. Coupling u_i in (16) is assumed to be linear and symmetric:

$$\mathbf{u} = \begin{pmatrix} u_0 \\ u_1 \\ \vdots \\ u_n \end{pmatrix} = \Gamma \begin{pmatrix} x_0 \\ x_1 \\ \vdots \\ x_n \end{pmatrix}, \ \Gamma = \gamma \begin{pmatrix} -n & 1 & \cdots & 1 \\ 1 & -n & \cdots & 1 \\ \cdots & \cdots & \cdots & \cdots \\ 1 & 1 & \cdots & -n \end{pmatrix}, \tag{17}$$

and parameter $\gamma \in \mathbb{R}_+$. Our choice of the coupling function in (17) is motivated by the following considerations. Fist, we wish to preserve the intrinsic dynamics of the neural oscillators when they synchronize, e.g. when $x_i = x_j$, $y_i = y_j$, $z_i = z_j$, $i, j \in \{0, \ldots, n\}$. For this reason it is desirable that the coupling vanishes when the synchronous state is reached. Second, we seek for a system in which synchronization between two arbitrary nodes, say the i-th and the j-th nodes, is determined exclusively by the degree of (mis)matches in $\phi_i(t)$, $\phi_j(t)$, independently of the activity of other units in the system. Third, the coupling should "pull" the system trajectories towards the synchronous state. Coupling function (17) satisfies all these requirements.

We set parameters of equations (16) to the following values:

$$\begin{array}{llll} a = 1, & b = 3, & c = 1, & d = 5, \\ s = 4, & x_0 = 1.6, & \epsilon = 0.001, & \end{array} \tag{18}$$

which correspond to the regime of chaotic bursting in each uncoupled element in (16) (Hansel & Sompolinsky, 1992).

The problem of detection of similarities in $\phi_0(t)$ and $\phi_i(t)$ can now be stated as follows.

Problem 2 (Detection) *Let system (16), (17) be given and there exist $i \in \mathcal{I}$ such that condition (12) is satisfied. Determine the coupling parameter γ as a function of system (16) parameters such that*

1) solutions of the system are bounded for all bounded ϕ_i, $i \in \mathcal{I}$;

2) states $(x_0(t), y_0(t), z_0(t))$ and $(x_i(t), y_i(t), z_i(t))$ asymptotically converge to a vicinity

of the synchronization manifold $x_0 = x_i$, $y_0 = y_i$, $z_0 = z_i$. *In particular,*

$$\limsup_{t\to\infty} |x_0(t) - x_i(t)| \le \delta(\varepsilon)$$
$$\limsup_{t\to\infty} |y_0(t) - y_i(t)| \le \delta(\varepsilon)$$
$$\limsup_{t\to\infty} |z_0(t) - z_i(t)| \le \delta(\varepsilon),$$

where $\delta(\cdot)$ *is a non-decreasing function vanishing at zero.*

In the next section we present solutions to the problems of invariance and detection. We start from considerations of what would be an adequate concept of analysis. The conclusion will be that for solving the problem of invariance, using the concept of Milnor attractors is advantageous over traditional concepts resting on the notion of Lyapunov stability. This implies that the sets to which the estimates $\hat{\theta}_{i,1}$, $\hat{\theta}_{i,2}$ converge should be weakly attracting rather than Lyapunov stable. We present a simple mechanism realizing this requirement for a wide class of models of disturbances. With respect to the second problem, that of detection, we provide sufficient conditions for asymptotic synchrony in system (16).

4 Main Results

Consider a system of temporal integrators, (13), in which the template subsystem (second equation in (13)) mimics the temporal code of an image as a result of applying adjustment mechanisms (14). Ideally, the template subsystem should have a single adjustment mechanism, which is structurally simple and yet capable of handling a broad class of perturbations. In addition it should require the least possible amount of a-priori information about images and templates.

In our search for a candidate adjustment mechanism let us first explore the available theoretical concepts which can be used in its derivation. The problem of invariance, as stated in Problem 1, can generally be understood as a specific optimization task. Particular solutions to such tasks as well as the choice of appropriate mathematical tools depend significantly on the following characteristics: uniqueness of the solutions, convexity with respect to parameters, and sensitivity to the input data (images and templates). Let us consider if the invariant template matching problem meets these requirements.

Uniqueness. Solutions to the problem of invariant template matching are generally *not unique*. The image may contain multiple instances of the template. Even if there is only a single unique object the template may fit it in multiple ways, for instance because it has rotational symmetry. Both cases are illustrated in Figure 4. A similar argument applies to

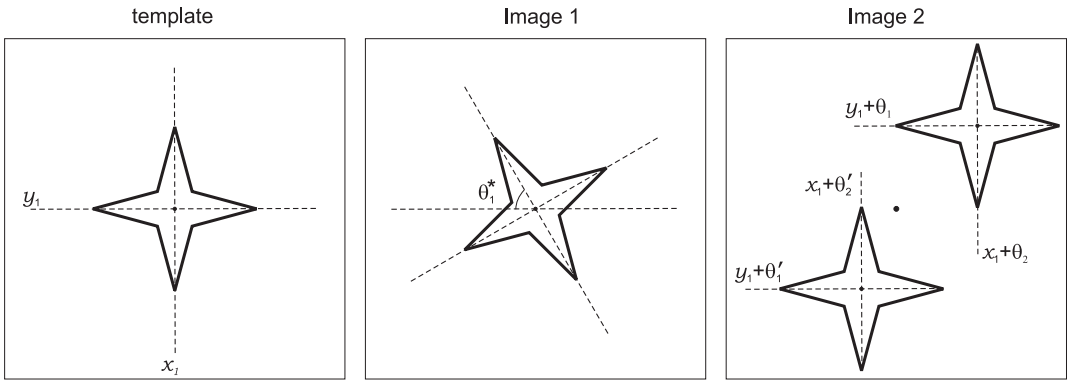

Figure 4: Example of a template and images which lead to non-unique solutions in the problem of invariant template matching. Image 1 is a rotated version of the template. Because the template has rotational symmetry, the angles $\theta_2 = \theta_2^* \pm \frac{\pi}{2}n$, $n = 0, 1, \ldots$ at which the template and the image match to each other are not unique. Image 2 contains two multiple instances of the template, which also leads to non-uniqueness.

translational invariance in the images with multiple instances of the template (right picture in Figure 4).

Non-linearity and non-convexity. The problem of invariant template matching is generally *nonlinear and nonconvex in* θ_1, θ_2. Nonlinearity is already evident from Table 1. For illustration of non-convexity consider the following function

$$\theta_1 f_i(t, \theta_2) = \theta_1 \int_{\Omega_{x,t} \times \Omega_{y,t}} e^{-|x-x_0|-|y-y_0|} \left(\int_{\Omega_x \times \Omega_y} e^{-\frac{1}{\theta_2}((x-\xi)^2+(y-\gamma)^2} S_i(\xi, \gamma) d\xi d\gamma \right) dxdy \quad (19)$$

which is a composition of Gaussian blur (the forth row in Table 1) with spatial sampling and subsequent exponential weighting (the second row in Table 2). In the literature on adaptive systems two versions of the convexity requirement are available. The first version applies to the case where the difference $\theta_1 f_i(t, \theta_2) - \hat{\theta}_{1,i} f_i(t, \hat{\theta}_{i,2})$ is not accessible for explicit measurement, and the variables $\phi_0(t)$, $\phi_i(t)$ should be used instead. In this case the convexity condition will have the following form (Fradkov, 1979):

$$\begin{aligned} e_i(\phi_0, \phi_i) \left[(\theta_1 - \hat{\theta}_{i,1}) \frac{\partial}{\partial \hat{\theta}_{i,1}} \hat{\theta}_{i,1} f_i(t, \hat{\theta}_{i,2}) + (\theta_2 - \hat{\theta}_{i,2}) \frac{\partial}{\partial \hat{\theta}_{i,2}} \hat{\theta}_{i,1} f_i(t, \hat{\theta}_{i,2}) \right] \geq \\ e_i(\phi_0, \phi_i) \left[\theta_1 f_i(t, \theta_2) - \hat{\theta}_{i,1} f_i(t, \hat{\theta}_{i,2}) \right] \end{aligned} \quad (20)$$

Term $e_i(\phi_0, \phi_i)$ in (20) is usually the difference $e_i(\phi_0, \phi_i) = \phi_0 - \phi_i$ and has the meaning of error. For the same pairs of points θ_1, θ_2 and $\hat{\theta}_{i,1}$, $\hat{\theta}_{i,2}$ condition (20) may hold or fail depending on the sign of $e_i(\phi_0(t), \phi_i(t))$ at the particular time instance t. Hence it is not always satisfied, not even for convex $\theta_{i,1} f_i(t, \theta_{i,2})$.

The second version of the convexity requirement applies when the difference $\theta_1 f_i(t, \theta_2) - \hat{\theta}_{i,1} f_i(t, \hat{\theta}_{i,2})$ can be measured explicitly. In this case the condition is formulated as definiteness of the Hessian of $\theta_1 f_i(t, \theta_2)$. It can easily be verified, however, that in (19) satisfaction of this requirement depends on the values of $S_i(\xi, \gamma)$. Hence both versions of the convexity conditions generally fail in invariant template matching.

Critical dependence on stimulation. An important feature of invariant template matching problem is that its solutions *critically depend* on particular images and templates. Presence of rotational symmetries in the templates affect the number of solutions. Hence objects with different numbers of symmetries will be characterized by sets of solutions with different cardinality.

We conclude that the problem of invariant template matching generally assumes multiple alternative solutions, nonlinearity and non-convexity with respect to parameters, and the structure of its solutions depends critically on a-priori unknown stimulation. What would be a suitable way to approach this class of problems in a principled manner?

Traditionally, processes of matching and recognition are associated with convergence of the system's state to an attracting set. In our case the system's state is defined by vector $\mathbf{x}$:

$$\mathbf{x} = (\phi_0, \phi_1, \ldots, \phi_i, \ldots, \hat{\theta}_{1,1}, \hat{\theta}_{2,1}, \ldots \hat{\theta}_{i,1}, \hat{\theta}_{i,2}, \ldots)$$

The attracting set, $\mathcal{A}$, is normally understood as a set satisfying the following definition (Guckenheimer & Holmes, 2002):

Definition 1 *A set $\mathcal{A}$ is an attracting set iff it is*

i) closed, invariant, and

ii) for some neighborhood $\mathcal{V}$ of $\mathcal{A}$ and for all $\mathbf{x}_0 \in \mathcal{V}$ the following conditions hold:

$$\mathbf{x}(t, \mathbf{x}_0) \in \mathcal{V} \ \forall \ t \geq 0; \tag{21}$$

$$\lim_{t \to \infty} \|\mathbf{x}(t, \mathbf{x}_0)\|_{\mathcal{A}} = 0 \tag{22}$$

Traditional techniques for proving attractivity employ the concept of Lyapunov asymptotic stability[6]. Although the notion of set attractivity is wider, the method of Lyapunov functions is constructive and, in addition, Lyapunov asymptotic stability implies the desired attractiviy. For these reasons it is highly practical, and the tandem of set attractivity in Definition 1 and Lyapunov stability has been used extensively in recognition systems, including Hopfield networks, recurrent neural nets, etc.

[6]We recall that the set $\mathcal{A}$ is (globally) Lyapunov asymptotically stable iff for all $\varepsilon > 0$ there exists $\delta(\mathbf{x}_0, \varepsilon) > 0$ such that $\|\mathbf{x}_0\|_{\mathcal{A}} < \delta(\mathbf{x}_0, \varepsilon) \Rightarrow \ \|\mathbf{x}(t, \mathbf{x}_0)\|_{\mathcal{A}} \leq \varepsilon$ for all $t \geq 0$, and $\lim_{t \to \infty} \|\mathbf{x}(t, \mathbf{x}_0)\|_{\mathcal{A}} = 0$

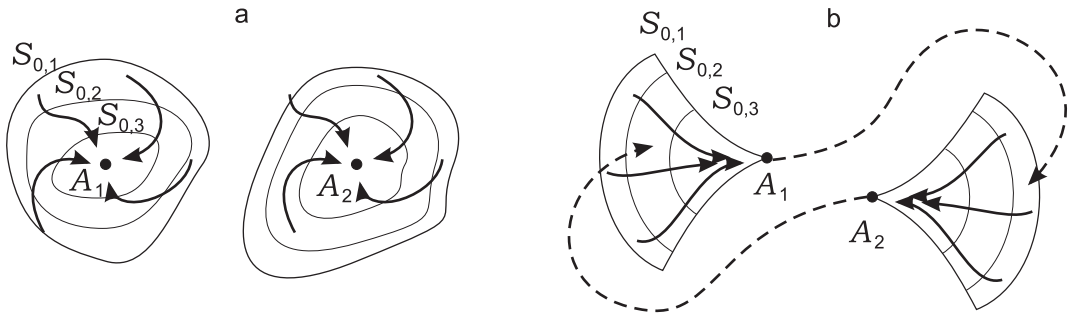

Figure 5: Standard stable attractors, panel a, vs weak attractors, panel b. Domains of stable attractors are neighborhoods containing $\mathcal{A}_1$, $\mathcal{A}_2$. Estimates of sizes of these domains depend on particular images $S_{0,1}$, $S_{0,2}$, $S_{0,3}$. These estimates are depicted as closed curves around $\mathcal{A}_1$, $\mathcal{A}_2$. Once the state converges to either of the attractors it stays there unless, probably, when the image changes. In contrast to this, domains of attraction for Milnor attracting sets are not neighborhoods. Hence, even a slightest perturbation in the image induces a finite probability of escape from the attractor. Hence multiple alternative representations of the image could eventually be recovered.

The problem of *invariant* template matching, however, challenges the universal appeal of this tandem. First, because of inherent non-uniqueness of the solutions, there are multiple invariant sets in the system's state space. Hence, global Lyapunov asymptotic stability cannot be ensured. Second, when each solution is treated as a locally stable invariant set, it is essentially important to know its domain of attraction. This domain, however, depends on properties of function $\theta_1 f_0(t, \theta_2)$ in (13), which vary with stimulation. Third, no method exists for solving Problem 1 for general nonlinearly parameterized $\theta_1 f_0(t, \theta_2)$ that assures Lyapunov stability of the system.

In order to solve the problem of invariant template matching we therefore propose to replace the standard notion of attracting set with a less restrictive concept. In particular we advocate the concept of weak or Milnor attracting sets (Milnor, 1985):

Definition 2 *A set $\mathcal{A}$ is weakly attracting, or Milnor attracting set iff*

i) it is closed, invariant and

ii) for some set $\mathcal{V}$ (not necessarily a neighborhood of $\mathcal{A}$) with strictly positive measure and for all $\mathbf{x}_0 \in \mathcal{V}$ limiting relation (22) holds

The main difference between the notions of a weak attracting set, Definition 2, and the standard one, Definition 1, is that the domain of attraction is not required to be a neighborhood of $\mathcal{A}$. The concept is illustrated in Figure 5. On the one hand, this allows us to use mathematical tools beyond the concept of Lyapunov stability in order to avoid problems with nonlinear parametrization and critical dependance on stimulation. On the other hand,

it offers a natural mechanism for systems to explore multiple image representations.

In the next paragraph we present technical details of how Problem 1 could be solved within the framework of Milnor attractors.

4.1 Invariant template matching by Milnor attractors

Consider system (13):

$$\begin{aligned}\dot{\phi}_0 &= -\frac{1}{\tau}\phi_0 + k \cdot \theta_1 f_0(t, \theta_2) \\ \dot{\phi}_i &= -\frac{1}{\tau}\phi_i + k \cdot \hat{\theta}_{i,1} f_i(t, \hat{\theta}_{i,2}),\ k, \tau \in \mathbb{R}_{>0},\ i \in \mathcal{I}\end{aligned}$$

and assume that the i-th template is present in the image. This implies that both the image and the template will have, at least locally in space, sufficiently similar spatiotemporal representations. Formally this can be stated as follows:

$$\exists\ \Delta \in \mathbb{R}_{>0} : \quad |\theta_1 f_0(t, \theta_2) - \theta_1 f_i(t, \theta_2)| \leq \Delta,\ \ \forall\ \theta_1, \theta_2,\ t \geq 0 \tag{23}$$

Hence without loss of generality we can replace equations (13) with the following:

$$\begin{aligned}\dot{\phi}_0 &= -\frac{1}{\tau}\phi_0 + k \cdot \theta_1 f_i(t, \theta_2) + \epsilon(t) \\ \dot{\phi}_i &= -\frac{1}{\tau}\phi_i + k \cdot \hat{\theta}_{i,1} f_i(t, \hat{\theta}_{i,2}),\ k, \tau \in \mathbb{R}_{>0},\ i \in \mathcal{I}\end{aligned} \tag{24}$$

where $\epsilon(t) \in L_\infty[0, \infty]$, $\|\epsilon(t)\|_\infty \leq \Delta$ is a bounded disturbance. Solving Problem 1, therefore, amounts to finding adjustment mechanisms (14) such that trajectories $\phi_0(t)$, $\phi_i(t)$ in (24) converge and limiting relations (15) hold.

The main idea of our proposed solution to this problem can informally be summarized as follows. First, we introduce an auxiliary system

$$\dot{\boldsymbol{\lambda}} = \mathbf{g}(\boldsymbol{\lambda}, \phi_0, \phi_i, t),\ \boldsymbol{\lambda} \in \mathbb{R}^\lambda,\ \mathbf{g} : \mathbb{R}^\lambda \times \mathbb{R} \times \mathbb{R} \times \mathbb{R}_{\geq 0} \to \mathbb{R}^\lambda \tag{25}$$

and define $\hat{\theta}_{i,1}$, $\hat{\theta}_{i,2}$ as functions of $\boldsymbol{\lambda}$, ϕ_0, and ϕ_i:

$$\hat{\theta}_{i,1} = \hat{\theta}_{i,1}(\boldsymbol{\lambda}, \tau, \kappa, \phi_0, \phi_i),\ \hat{\theta}_{i,2} = \hat{\theta}_{i,2}(\boldsymbol{\lambda}, \tau, \kappa, \phi_0, \phi_i). \tag{26}$$

Second, we show that for some $\varepsilon \in \mathbb{R}_{>0}$, and $\Omega_\lambda \subset \mathbb{R}^\lambda$ the following set

$$\Omega^* = \{\phi_0, \phi_i \in \mathbb{R}, \boldsymbol{\lambda} \in \mathbb{R}^\lambda |\ |\phi_0(t) - \phi_i(t)| \leq \varepsilon,\ \boldsymbol{\lambda} \in \Omega_\lambda \subset \mathbb{R}^\lambda\}$$

is forward-invariant in the extended system (24), (25) and (26). Third, we restrict our attention to systems which have a subset Ω in their state space such that trajectories starting

in Ω converge to Ω^*. Finally, we guarantee that the state will eventually visit domain Ω thus ensuring that (12) holds.

We have found that choosing extension (25) in the class of simple third-order bilinear systems

$$\begin{cases} \dot{\lambda}_1 = \dfrac{\gamma_1}{\tau} \cdot (\phi_0 - \phi_i) \\ \dot{\lambda}_2 = \gamma_2 \cdot \lambda_3 \cdot \|\phi_0 - \phi_i\|_\varepsilon, \quad \gamma_1, \gamma_2 \in \mathbb{R}_{>0} \\ \dot{\lambda}_3 = -\gamma_2 \cdot \lambda_2 \cdot \|\phi_0 - \phi_i\|_\varepsilon, \quad \sqrt{\lambda_2^2(t_0) + \lambda_3^2(t_0)} = 1 \end{cases} \tag{27}$$

ensures the solution of Problem 1. Specific technical details and conditions are provided in Theorem 1

Theorem 1 *Let system (24), (27) be given, and function $f_i(t, \theta_2)$ be separated from zero and bounded. In other words, there exist constants $D_3, D_4 \in \mathbb{R}_{>0}$ such that for all $t \geq 0$, $\theta_2 \in [\theta_{2,\min}, \theta_{2,\max}]$ the following condition holds:*

$$D_3 \leq f_i(t, \theta_2) \leq D_4 \tag{28}$$

Then there exist positive γ_1, γ_2, and ε (see Table 3 for the particular values):

$$\gamma_2 \ll \gamma_1, \quad \varepsilon > \tau\Delta \left(1 + \frac{D_4}{D_3}\right) \tag{29}$$

such that adaptation mechanisms

$$\begin{cases} \hat{\theta}_{i,1} = e_i\gamma_1 + \lambda_1 \\ \hat{\theta}_{i,2}(t) = \theta_{2,\min} + (\lambda_2(t) + 1)\, \dfrac{\theta_{2,\max} - \theta_{2,\min}}{2} \end{cases} \tag{30}$$

deliver a solution to Problem 1. In particular, for all $\theta_1 \in [\theta_{1,\min}, \theta_{1,\max}]$, $\theta_2 \in [\theta_{2,\min}, \theta_{2,\max}]$ the following properties are guaranteed:

$$\limsup_{t\to\infty} |\phi_0(t) - \phi_i(t)| \leq \varepsilon; \quad \exists\ \theta_2' \in [\theta_{2,\min}, \theta_{2,\max}] : \ \lim_{t\to\infty} \hat{\theta}_{i,2}(t) = \theta_2',$$

where the value of ε, depending on the choice of parameters γ_2, γ_1, can be made arbitrarily close to $\tau\Delta\,(1 + D_4/D_3)$.

Proof of the theorem is provided in Appendix 2.

Let us comment on the conclusions and conditions of Theorem 1. First of all, the theorem shows that each i-th subsystem ensuring invariance of a spatiotemporal image representation to the given modelled perturbations can be composed of no more than four differential

Table 3: Parameters of the compensatory mechanisms (30)

Parameter	Values
γ_1	$\frac{\gamma_1}{\gamma_2} = q,\ q \in \mathbb{R}_{>0}$
ε	$\varepsilon > \tau\left(\Delta\left(1+\frac{D_4}{D_3}\right)+\frac{\gamma_2}{\gamma_1}\left[\frac{\theta_{1,\max}DD_2D_4}{(D_3)^2}M_1\tau\left(1+\frac{D_4}{D_3}\right)\frac{\theta_{2,\max}-\theta_{2,\min}}{2}\right]\right)$ $M_1 = \Delta + k\theta_{1,\max}DD_2\lvert\theta_{2,\max}-\theta_{2,\min}\rvert$
γ_2	$\gamma_2 < \left(\frac{1}{4\tau}\right)^2\left[k\theta_{1,\max}DD_2\left(1+\frac{D_4}{D_3}\right)\left(\frac{\theta_{2,\max}-\theta_{2,\min}}{2}\right)\right]^{-1}$

equations:

$$\text{Temporal integration :} \qquad \dot{\phi}_i = -\frac{1}{\tau}\phi_i + k\cdot\hat{\theta}_{i,1}f_i(t,\hat{\theta}_{i,2}) \tag{31a}$$

$$\text{Fast adaptation dynamics :} \qquad \dot{\lambda}_1 = \frac{\gamma_1}{\tau}\cdot(\phi_0-\phi_i) \tag{31b}$$

$$\text{Slow adaptation dynamics :} \qquad \begin{cases} \dot{\lambda}_2 &= \gamma_2\cdot\lambda_3\cdot\|\phi_0-\phi_i\|_\varepsilon, \\ \dot{\lambda}_3 &= -\gamma_2\cdot\lambda_2\cdot\|\phi_0-\phi_i\|_\varepsilon \end{cases} \tag{31c}$$

Notice that the time scales of temporal integration (31a), adaptation to linearly parameterized uncertainties, (31b), and adaptation to nonlinearly parameterized uncertainties, (31c), are all different. Because of these differences, subsystem (31b) is referred to as *slow adaptation dynamics* and subsystem (31c) as *fast adaptation dynamics*. The difference between their time scales determines the degree of invariance and precision in the resulting system. For instance, as follows from Table 3, the ratio γ_2/γ_1 affects the value of ε. This value defines the acceptable level of mismatches between an image and a template. In other words, it regulates the sensitivity of the system. The smaller the ratio γ_2/γ_1, the higher the sensitivity. Ratio $\gamma_2/(1/\tau)$ (see proof for details) affects the conditions for convergence.

The slow adaptation dynamics, (31c), can be interpreted as a *searching, or wandering* dynamics in the interval $[\theta_{2,\min},\theta_{2,\max}]$. Its function is to explore the interval $[\theta_{2,\min},\theta_{2,\max}]$ for possible values of $\hat{\theta}_{i,2}$ when models of perturbation are inherently nonlinear and no other choice except of explorative search is available. Solutions of the searching dynamics in (31c) are harmonic signals with time-varying frequency $\gamma_2\|\phi_0(t)-\phi_i(t)\|_\varepsilon$. The larger the error,

the higher the frequency of oscillation. When $\gamma_2\|\phi_0(t) - \phi_i(t)\|_\varepsilon$ is constant, for instance equals to unit, equations (31c) reduce to

$$\begin{aligned} \dot{\lambda}_2 &= \lambda_3 \\ \dot{\lambda}_3 &= -\lambda_2 \end{aligned} \tag{32}$$

We presently adopt (32) as a prototype system for generating searching trajectories. This is motivated primarily by its simplicity in realization and linearity in state. In general, every system

$$\begin{aligned} \dot{\lambda}_2 &= g_2(\lambda_2, \lambda_3, t), \\ \dot{\lambda}_3 &= g_3(\lambda_2, \lambda_3, t), \quad g_2, g_3 \in C^0 \end{aligned} \tag{33}$$

generating dense trajectories $\lambda_2(t)$ in $[\theta_{2,\min}, \theta_{2,\max}]$ for some initial conditions $\lambda_2(t_0)$, $\lambda_3(t_0)$ and at the same time ensuring boundedness of $\lambda_2(t)$, $\lambda_3(t)$ for all $t \in \mathbb{R}_{\geq 0}$ could replace (32) in (31c), see also (Tyukin et al., 2008). Conclusions of the theorem in this case will remain the same except of the values of γ_1, γ_2, ε in Table 3.

The fast adaptation dynamics, (31b), corresponds to exponentially stable mechanisms. This can easily be verified by differentiating the difference $\hat{\theta}_{i,1}(t) - \theta_1$ with respect to time (see also (51) in Appendix 2). The function of the fast adaptation subsystem is to track instantaneous changes in θ_1 exponentially fast in such a way that the difference $\hat{\theta}_{i,1}(t) - \theta_1$ is determined mostly by mismatches $\hat{\theta}_{i,2}(t) - \theta_2$.

The problem of template matching is solved through the interplay of searching dynamics $\hat{\theta}_{i,2}(t) - \theta_2$ (see Figure 6) and the stable, contracting dynamics expressed by $\phi_0(t) - \phi_i(t)$. We use the results from (Tyukin et al., 2008) to prove the emergence of weakly (Milnor) attracting sets in the system state space.

In principle, linearity of the uncertainty models in θ_1 is not necessary to guarantee exponential stability of $\hat{\theta}_{i,1}(t) - \theta_1$. As has been shown in (Tyukin et al., 2007), exponential stability of $\hat{\theta}_{i,1}(t) - \theta_1$ can be ensured by the same function $\hat{\theta}_{i,1}(t)$ as in (26) if we replace $\theta_1 f_i(t, \theta_2)$ with $\tilde{f}_i(t, \theta_1, \theta_2) : \mathbb{R}_{\geq 0} \times \mathbb{R} \times \mathbb{R} \to \mathbb{R}$. Nonlinearities $\tilde{f}_i(t, \theta_1, \theta_2)$, however, should be monotone in θ_1. In this case condition (28) is to be replaced with the following

$$D_3 \leq \frac{\tilde{f}_i(t, \hat{\theta}_{i,1}, \theta_2) - \tilde{f}_i(t, \theta_1, \theta_2)}{\hat{\theta}_{i,1} - \theta_1} \leq D_4, \ \forall\ \theta_2 \in [\theta_{2,\min}, \theta_{2,\max}] \tag{34}$$

The general line of the proof remains unaffected by this extension.

The proposed compensatory mechanisms (24), (27) (30) are nearly optimal in terms of the dimension of the state of the whole system. Indeed, in order to track uncertain and independent θ_1, θ_2 two extra variables are to be introduced. The minimal dimension of the

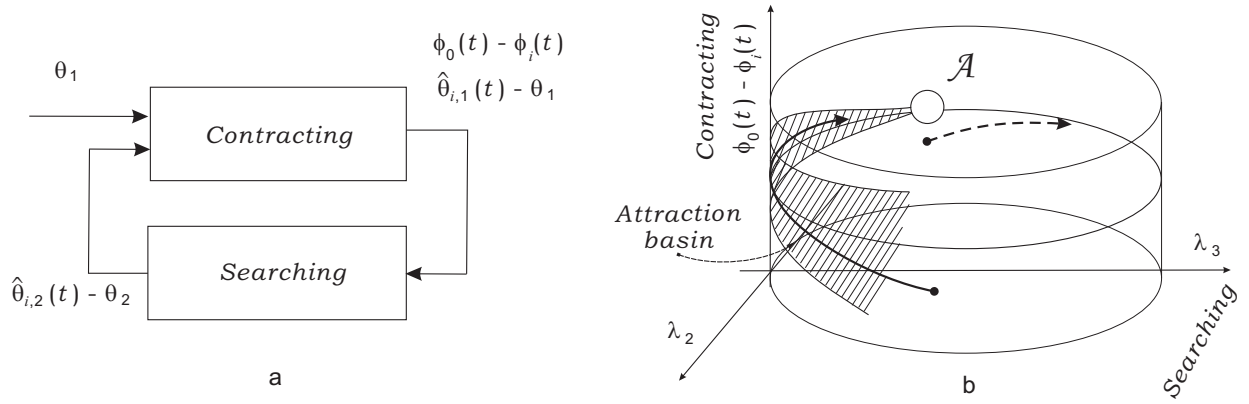

Figure 6: The interplay between temporal integration, (31a), and fast and slow adaptation (31b), (31c) in the proposed solution to the problem of invariant template matching. **Panel a.** Contracting dynamics corresponds to the processes of temporal integration of a template and adaptation to linearly parameterized uncertainties. Searching dynamics corresponds to the adaptation to nonlinearly parameterized uncertainties. **Panel b.** Diagram of the phase portrait of system (31a), (31b), (31c). Interaction between searching and contracting subsystems forms a weakly attracting invariant set $\mathcal{A}$. Its basin of attraction is not necessarily a neighborhood of $\mathcal{A}$. This means that some trajectories starting in a small vicinity of $\mathcal{A}$ may eventually leave its neighborhood (dashed trajectory), while trajectories starting far away from $\mathcal{A}$ enter such neighborhoods and remain there (solid line).

state of a system which solves Problem 1 equals three. This implies that our four-dimensional system is close to the optimal configuration. Furthermore, as follows from the proof of the theorem, the dimension of the slow subsystem could be reduced to one. Thus, in principle, a minimal realization could be achieved. In this case, however, boundedness of the state for every initial condition is no longer guaranteed.

Theorem 1 establishes convergence conditions for the trajectories of our prototype system (24), (27) (30) to an invariant set in the system state space. In particular, when matching condition (23) is met, the theorem assures that temporal representation $\phi_i(t)$ of the template tracks temporal representation $\phi_0(t)$ of the image. In the next subsection we discuss how the similarity between these temporal representations can be detected by a system of coupled spiking oscillators. In particular, we will consider coincidence detectors (16), (17), (18) modeled by a system of coupled Hindmarsh-Rose oscillators.

4.2 Conditions for synchronization of coincidence detectors

The goal of this section is to provide a constructive solution to Problem 2, the problem of detection. First, we seek for conditions ensuring global exponential stability of the synchronization manifold of $\phi_0(t) = \phi_i(t)$ when $\phi_i(t)$ are identical for each i. We do this by

showing that solutions of the system are globally bounded, and for each pair of indexes $i, j \in \{0, \ldots, n\}$ there exists a differentiable positive definite function $V(x_i, y_i, z_i, x_j, y_j, z_j)$, $\partial V/\partial x_i = -\partial V/x_j$ such that V grows towards infinity with distance from the synchronization manifold and for all bounded continuous $\phi_i(t) = \phi_j(t)$ the following holds:

$$\dot{V} \leq -\alpha V, \ \alpha \in \mathbb{R}_{>0}. \tag{35}$$

When $\phi_i(t) \neq \phi_j(t)$ equation (35) implies that

$$\dot{V} \leq -\alpha V + \frac{\partial V}{x_i}(\phi_i(t) - \phi_j(t)). \tag{36}$$

Then using (36) and the Comparison Lemma (Khalil, 2002), we show that convergence of $\phi_i(t)$ to $\phi_j(t)$ at $t \to \infty$ implies convergence of variables $x_i(t)$, $y_i(t)$, $z_i(t)$, $x_j(t)$, $y_j(t)$, $z_j(t)$ to the synchronization manifold. The formal statement of this result is provided in Theorem 2

Theorem 2 *Let system (16) be given, function* $\mathbf{u}$ *be defined as in (17) and functions* $\phi_i(t)$, $i \in \{0, \ldots, n\}$ *be bounded. Then*

1) solutions of the system are bounded for all $\gamma \in \mathbb{R}_+$*;*

2) if, in addition, the following condition is satisfied

$$\gamma > \frac{1}{(n+1) \cdot a} \left(\frac{d^2}{2} + b^2 \right), \tag{37}$$

then for all $i, j \in \{0, \ldots, n\}$ *condition*

$$\limsup_{t \to \infty} |\phi_i(t) - \phi_j(t)| \leq \varepsilon$$

implies that

$$\begin{aligned} \limsup_{t \to \infty} |x_i(t) - x_j(t)| &\leq \delta(\varepsilon), \\ \limsup_{t \to \infty} |y_i(t) - y_j(t)| &\leq \delta(\varepsilon), \\ \limsup_{t \to \infty} |z_i(t) - z_j(t)| &\leq \delta(\varepsilon). \end{aligned} \tag{38}$$

where $\delta : \mathbb{R}_+ \to \mathbb{R}_+$ *is a monotone function vanishing at zero.*

Theorem 2 specifies the boundaries for stable synchrony in the system of coupled neural oscillators (16) as a function of the coupling strength, γ, and parameters a, b, and d of a single oscillator. The last three parameters represent properties of the membrane and combined with x_0, ε, s and I completely characterize the dynamics of a single model neuron (Hindmarsh & Rose, 1984), ranging from single spiking to periodic or chaotic bursts.

The distinctive feature of Theorem 2 is that it is suitable for analysis of systems with external time-dependent perturbations $\phi_i(t)$. This property is essential for the comparison task, where the oscillators are fed with time-varying inputs and the degree of their mutual synchrony is the measure of similarity between the inputs.

While the theorem provides us with conditions for stable synchrony, it allows us to estimate the domain of values of the coupling parameter γ corresponding to potential intermittent, itinerant (Kaneko & Tsuda, 2000, 2003), or meta-stable regimes. In particular, as follows from Theorem 2, a necessary condition for unstable synchronization in system (16) is

$$\gamma < \frac{1}{(n+1)\cdot a}\left(\frac{d^2}{2} + b^2\right). \tag{39}$$

Notice that conditions (39), (37) do not depend on the "bifurcation" parameter I which usually determines the type of bursting in the single oscillator. They also do not depend on the differences in the time scales defined by parameter ε between the fast x, y, and slow, z, variables. Hence these conditions apply in a wide range of system behavior on the synchronization manifold. This advantage also has a downside, because conditions (39), (37) are too conservative. However, this may be a reasonable price for invariance of criteria (39), (37) with respect to the full range of dynamical behavior of a generally nonlinear system.

5 Discussion

We provided a principled solution to the problem of invariant recognition in template matching. Recognition occurs when mismatches in the temporal representations of image and templates converge to a small neighborhood of zero. This in turn leads to synchronized trajectories in a network of nonlinear oscillators serving as detectors of coincidences. Although our overall implementation of this idea may not normative we tried to keep the number of relevant parameters at minimum. In particular the dimension of the state of a single adaptation compartment is three, which is minimal for generation of spikes ranging from periodic to chaotic bursts. Moreover, conditions (39), (37) allow us to choose coupling strength γ as a single control parameter for regulating stability/instability of the synchronous activity in the network.

In this section we provide further extensions of the basic results of Theorems 1, 2, discuss possible links between the normative part of our theory and some known results in biological, human vision.

5.1 Extension to the frequency-encoding schemes

For the sake of notational simplicity we restricted our attention to temporal representations (6), (9) of spatially sampled images. These encoding schemes can be interpreted as scanning of an image over time. Yet, the results of Section 4 apply to a broader class of encoding schemes. One example is frequency-coding used in many neural systems. Let us consider factorization (6) where in the notation $\mathcal{F}_t[S_0, \boldsymbol{\theta}](x, y)$ symbol t is replaced with ν. In order to extend the initial encoding scheme to the domain of frequency/spike rate encoding we introduce an additional linear functional f_ω as follows:

$$f_\omega(t, \mathcal{F}_\nu[S_0, \boldsymbol{\theta}]) = \sum_\nu h(\omega_\nu \cdot t) \cdot f(\mathcal{F}_\nu[S_0, \boldsymbol{\theta}]), \tag{40}$$

where $h : \mathbb{R} \to \mathbb{R}$ is a bounded periodic function, and ω_ν are distinct real numbers indexed by ν. Function $h(\omega_\nu \cdot t)$ in (40) serves as a basis or carrier function generating periodic impulses of various frequencies ω_ν. Thus each ν-th spatial sample of the image is assigned a particular frequency, and the amplitude of the oscillation is specified by $f(\mathcal{F}_\nu[S_0, \boldsymbol{\theta}])$. Temporal representation of a one-dimensional stimulus according to encoding scheme (40) is illustrated in Figure 7, panel a.

This encoding scheme is plausible to biological vision, when frequencies ω_ν are ordered according to relative position of domains $\Omega_{x,\nu}$, $\Omega_{y,\nu}$ to the center of the image. This corresponds, in particular, to the receptive fields in cat retinal ganglion cells (Enroth-Cugell et al., 1983). Because the functional f_ω is linear in $f(\mathcal{F}_\nu[S_0, \boldsymbol{\theta}])$ and function $h(\omega_\nu \cdot t)$ is bounded for all t, condition (8) will be satisfied for f_ω. Hence the conclusions of Theorem 1 apply to these representations.

5.2 Multiple representations of uncertainties

Another property of system (24), (27), (30), in addition to its ability to accommodate relevant encoding schemes such as frequency/rate and sequential/random scanning, is that each single value of $\theta_2 \in (\theta_{2,\min}, \theta_{2,\max})$ induces at least two distinct attracting sets in the extended space. Indeed

$$\lambda_2^2(t) + \lambda_3^2(t) = \text{const} = 1$$

along the trajectories of (24), (27), (30) (see also the proof of Theorem 1). Hence for almost every value of λ_2 (except when $\lambda_2 = \pm 1$) in the definition of $\hat{\theta}_2(t)$ in (30) there will always be two distinct values of λ_3:

$$\lambda_{3,1} = \sqrt{1 - \lambda_2^2},\ \lambda_{3,2} = -\sqrt{1 - \lambda_2^2}.$$

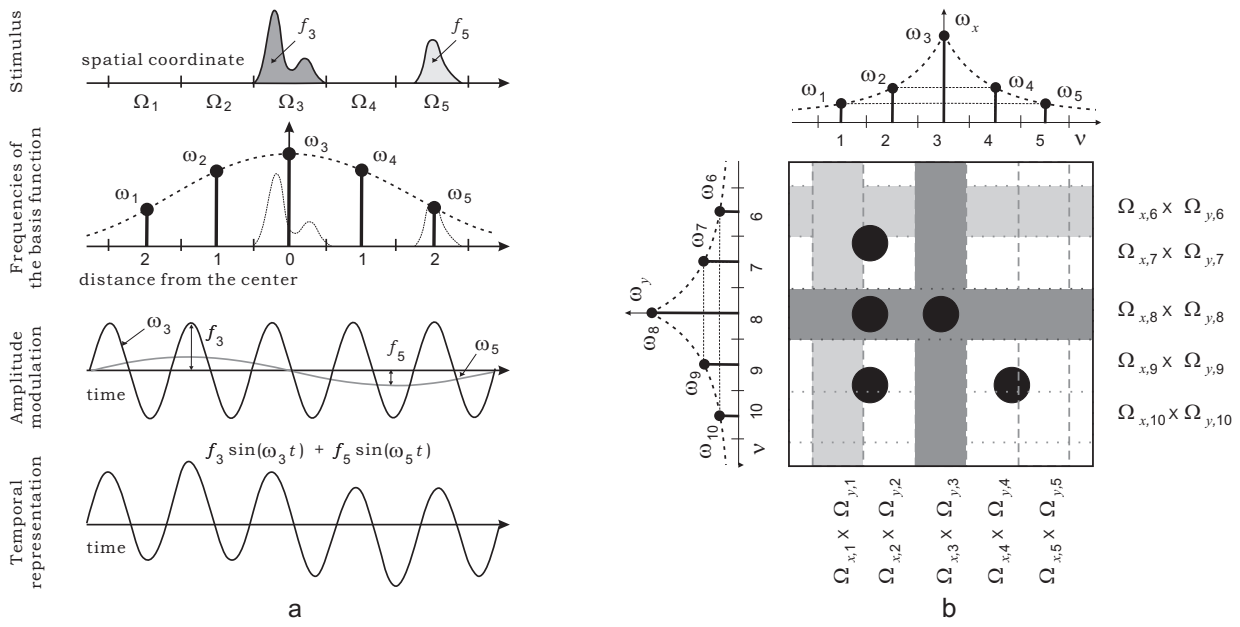

Figure 7: **Panel a.** Temporal representation of a spatially distributed stimulus using frequency encoding. A stimulus (upper row) $S(x)$ is spatially sampled by partitioning its domain into the union of intervals Ω_i. For each Ω_i an integral $f_i = f(\mathcal{F}_i) = \int_{\Omega_i} S(x)dx$ is calculated and a frequency ω_i is assigned. The resulting temporal representation (lower row) is expressed as the sum of two amplitude-modulated harmonic signals of frequencies, ω_3, ω_5. **Panel b.** Temporal representation of a two-dimensional pattern. The pattern consists of black filled circles. The image domain is partitioned into a collection of horizontal and vertical strips. Darker domains correspond to higher frequencies.

These two values give rise to distinct invariant sets in the system state space for a single value of θ_2. The presence of two complementary encodings for the same figure is a plausible assumption that has been used in the perceptual organization literature to explain a range of phenomena, including perceptual ambiguity, modal and amodal completion, etc. (Hatfield & Epstein, 1985), (Leeuwenberg & Buffart, 1983), p. 29, (Shepard, 1981). A consequence of the presence of multiple attractors corresponding to the single value of perturbation is that the time for convergence (the decision time) may change abruptly with small variations of initial conditions. The latter property is well documented in human subjects (Gilden, 2001). Furthermore, the presence of two attractors with different basins for a single value of perturbation will lead to asymmetric distributions of decision times, which is typically observed in human and animal reaction time data (Smith & Ratcliff, 2004).

5.3 Multiple time scales for different modalities in vision

An important property of the proposed solution to the problem of invariance is that the time scales of adaptation to linearly and nonlinearly parameterized uncertainties are substantially

different. This difference in time scales emerged naturally in the course of our mathematical argument as a consequence of splitting the system dynamics into a slow searching subsystem and a fast asymptotically stable one. This allowed us to prove emergence of unstable yet attracting invariant sets, thus ensuring existence of a solution to the problem of invariant template matching. In particular, Theorem 1 requires that the time constant of adaptation to image intensity (a linearly parameterized uncertainty) is substantially smaller than those of image blur, rotation, or scaling (nonlinearly parameterized uncertainties). Indeed, as follows from Table 3, the larger the difference in the time scales the higher the possible precision and the smaller the errors. This is not to say that successful adaptation is impossible if the time scales of adaptation are of the same order. Our results are sufficient and only suggest that having different adaptation time scales may be beneficial for convergence. On the other hand, a simple geometrical argument can be used to demonstrate that the larger the value of γ_1/τ the larger the trapping regions of stimuli-induced attracting sets (Gorban et al., 2008). In Section 6.1.3 we illustrate with an example how the time scales of adaptation to different modalities might affect performance of a simple recognition system.

Even though the difference in time scales was motivated purely by theoretical considerations, there is strong evidence that biological systems adapt at different time scales to uncertainties from different modalities. For example, the time scale of light adaptation is within tens of milliseconds (Wolfson & Graham, 2000) while adaptation to "higher-order" modalities such as rotation and image blur extends from hundreds of milliseconds to minutes (Webster et al., 2002). In motor learning evidence for the presence of slow and fast adaptation is reported in (Smith et al., 2006). These findings, therefore, motivate our belief that system (24), (27), (30) could serve as a simple, yet qualitatively realistic, model for adaptation mechanisms in vision, motor behavior, and decision making.

6 Examples

In this section we provide simple illustrations of how particular systems for invariant template matching can be constructed using the results of this article.

6.1 Rotation-invariant matching and mental rotation experiments

Let us illustrate how the results of Theorems 1, 2 can be applied to template matching when an object is rotated over an unknown angle and its brightness is uncertain a-priori. Below we consider three examples illustrating the performance of our system in different experimental settings. The first example corresponds to the case when only one object is present in the

image. The task is to detect the object and infer its rotation angle and brightness. In the second example we consider an image which contains two different objects of which the rotation angle and brightness are uncertain. The system should be able to report matching templates and estimate the values of rotation angles and brightness. In the third experiment we illustrate the importance of separating the adaptation time scales.

6.1.1 Rotation-invariant matching in images with single objects

Without loss of generality and for the sake of notational convenience, suppose that the domain $\Omega_x \times \Omega_y$ is a square of the following dimensions: $\Omega_x \times \Omega_y = [0, y_{\max}] \times [0, x_{\max}]$. In order to obtain a temporal representation of the image we use the frequency-encoding scheme (40) which was illustrated in Figure 7, panel b. In particular we use the following transformation

$$\theta_1 f_i(t, \theta_2) = \theta_1 \sum_{\nu} h(\omega_\nu \cdot t) \cdot f(\bar{\mathcal{F}}_\nu[S_i, \theta_2]), \tag{41}$$

where θ_2 is the rotation angle of image $S_i(x, y)$ around its central point, θ_1 is the image brightness, function $h(\omega_\nu \cdot t) = \sin^2(\omega_\nu \cdot t)$, and

$$f(\bar{\mathcal{F}}_\nu[S_i, \theta_2]) = \int_{\Omega_{x,\nu} \times \Omega_{y,\nu}} \bar{\mathcal{F}}_\nu[S_i, \theta_2](\xi, \gamma) d\xi d\gamma. \tag{42}$$

is simply an integral of the rotated image S_i by an angle θ_2 over the strip $\Omega_{x,\nu} \times \Omega_{y,\nu}$.

For instance, let us have m horizontal strips aligned along the x-coordinates of the templates, and n vertically aligned strips along the y-coordinates. Then

$$\Omega_{x,i} \times \Omega_{y,i} = \begin{cases} [a(i), b(i)] \times [0, y_{\max}], & a(i) < b(i),\ i = 1, \ldots, m \\ [0, x_{\max}] \times [a(i), b(i)], & a(i) < b(i),\ i = m+1, \ldots, m+n \end{cases},$$

and integrals (42) transform into

$$f(\bar{\mathcal{F}}_\nu[S_i, \theta_2]) = \begin{cases} \int_{a(\nu)}^{b(\nu)} \int_{0}^{y_{\max}} \bar{\mathcal{F}}_\nu[S_i, \theta_2](\xi, \gamma) d\xi d\gamma, \nu = 1, \ldots, m \\ \int_{0}^{x_{\max}} \int_{a(\nu)}^{b(\nu)} \bar{\mathcal{F}}_\nu[S_i, \theta_2](\xi, \gamma) d\xi d\gamma, \nu = m+1, \ldots, m+n \end{cases} \tag{43}$$

Hence our temporal representation of the image and the templates is simply a weighted sum of periodic functions of time $\sin^2(\omega_\nu \cdot t)$, scaled by θ_1, with weights determined by (43).

According to (24), (27), (30), (16) the recognition system (see Figures 3, 9 for its general structure) can be described by the system of differential equations provided in Table 4. Implementation details, initial conditions, and the source files of a working MATLAB Simulink model can be found in (Tyukin et al., 2007).

Function	Image	Template
Temporal integration	$\dot{\phi}_0 = -\frac{1}{\tau}\phi_0 + k \cdot \theta_1 f(t, \theta_2)$	$\dot{\phi}_i = -\frac{1}{\tau}\phi_i + k \cdot \hat{\theta}_{1,i} f(t, \hat{\theta}_{2,i})$
Adaptation to brightness	No	$\hat{\theta}_{1,i} = (\phi_0 - \phi_i)\gamma_1 + \lambda_{i,1}$ $\dot{\lambda}_{i,1} = \frac{\gamma_1}{\tau}(\phi_0 - \phi_i)$
Adaptation to rotation	No	$\hat{\theta}_{2,i} = (\lambda_{2,i}(t) + 1)\pi$ $\dot{\lambda}_{i,2} = \gamma_2 \lambda_{i,3} \|\phi_0 - \phi_i\|_\varepsilon$ $\dot{\lambda}_{i,3} = -\gamma_2 \lambda_{i,2} \|\phi_0 - \phi_i\|_\varepsilon$
Detectors of similarity	$\dot{x}_0 = -ax_0^3 + bx_0^2 + y_0 - z_0 + I + u_0 + \phi_0(t)$, $\dot{y}_0 = c - dx_0^2 - y_0$, $\dot{z}_0 = \epsilon(s(x_0 + \bar{x}_0) - z_0)$,	$\dot{x}_i = -ax_i^3 + bx_i^2 + y_i - z_i + I + u_i + \phi_i(t)$, $\dot{y}_i = c - dx_i^2 - y_i$, $\dot{z}_i = \epsilon(s(x_i + \bar{x}_0) - z_i)$,
Coupling function	$u_0 = \gamma\left(-(N+1)x_0 + \sum_{j\neq 0} x_j\right)$	$u_i = \gamma\left(-(N+1)x_i + \sum_{j\neq i} x_j\right)$
Parameters	Temporal integration subsystem: $\tau = 1$, $\theta_1 = 2.3$, $\theta_2 = \pi/4$, $k = 1/20$, $x_{\max} = 101$, $y_{\max} = 101$, $m = 33$, $n = 17$, $a(i) = 1, 4, 7, \ldots, 101 - 3$, $\omega_i = 1/80$ $i \leq m$; $a(i + m) = 1, 7, 13, \ldots$, $\omega_{i+m} = 1/30$, $i \leq n$, $b(i) = a(i) + 3$, Detectors of similarity: $a = 1$, $b = 3$, $c = 1$, $d = 5$, $\epsilon = 0.001$, $s = 4$, $\gamma = 0.5$, $I = -6.2$, $\bar{x}_0 = 1.6$	Intensity adaptation subsystem: $\gamma_1 = 0.5$ Rotation adaptation subsystem: $\gamma_2 = 0.01$, $\varepsilon = 0.05$

Table 4: Equations of the system for rotation and brightness-invariant template matching; N – the total number of templates.

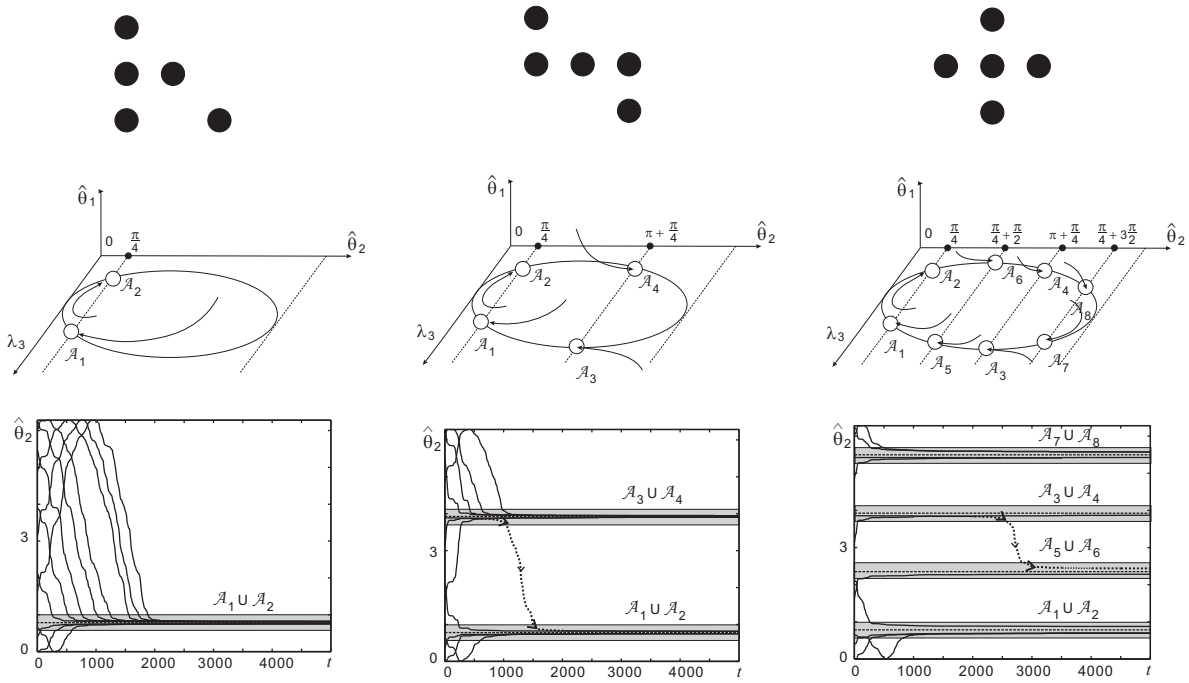

Figure 8: Template matching for Garner patterns with 3 levels of complexity. The patterns (upper row) were rotated by $\pi/4$ and varied in intensity levels. Depending on the number of their rotational symmetries they induced different numbers of invariant sets in the system state space: two, four and eight respectively. The diagrams of corresponding phase plots are provided in the middle row. Estimates of the rotation angle as functions of time for different initial conditions are depicted in the third row.

We tested system performance for a variety of input images, in particular the class of Garner patterns (Garner, 1962) (see Figure 8, first row; for ease of computation we used relatively low resolution images of 101×101, i.e. with $x_{\max}, y_{\max} = 101$). These patterns serve as a interesting benchmark because in a long line of behavioral experiments, most recently (Lachmann & van Leeuwen, 2005), the human pattern recognition process of these patterns has been studied in great detail. Overall intensity of these patterns does not vary from one pattern to another. At the same time, the number of symmetries increases from the first, through the second to the third pattern in Figure 8. Because of this, their complexity decreases proportionally (Garner, 1962).

Using as templates the first row of Figure 8, we developed and ran a recognition system, of which the description is given in Table 4. The second row of Figure 8 illustrates the system dynamics involved in template matching. The diagrams represent phase plots of the successful node j (for the template subsystem in which the matching occurs). The third row contains trajectories of the estimates of the rotation angle $\hat{\theta}_{j,2}(t)$. Each object induces

various number of invariant sets in the template subsystems. The number of these invariant sets is inversely proportional to stimulus complexity. Hence, the higher the complexity the more time the system requires to reach one. Thus the time needed for recognition increases monotonically with the stimulus complexity. This is consistent with empirical results reported in experimental studies, for instance (Lachmann & van Leeuwen, 2005).

An additional property of our system is that it is capable of reporting multiple representations of the same object. This is indicated by the dashed trajectories in Figure 8. Even though the system parameters are chosen such that trajectories converge to an attractor, we can still observe meta-stable behavior. This is because the attractors in our system are of Milnor-type, which implies that trajectories starting in the vicinity of one attractor may actually belong to the basin of another attractor. Furthermore, it is even possible to tune the system in such a way that it will always switch from one representation to another. The latter property suggests that our simple system in Table 4 can model perceptual ambiguity and binocular rivalry, where spontaneous switching and perceptual multi-stability are commonly observed (Attneave, 1971; Leopold & Logothetis, 1999).

6.1.2 Rotation-invariant matching in images with multiple objects

Let us now consider the case in which two patterns are simultaneously present in an image. As an image we chose a concatenation of two rotated Garner patterns. The values of rotation angles and intensity of the patterns are unknown. In order to be able to detect and recognize multiple patterns in the image, the system, in addition to ensuring rotation and intensity adaptation, should be able to scan the image in space. Therefore we extend the system for invariant template matching as proposed in the previous subsection (see Table 4) by introducing an additional operation, i.e. a (moving) frame, which projects part of the image into a spatiotemporal code, similarly to (41). In particular, instead of (41)–(43) we will deal with the following spatiotemporal representation

$$\theta_1 f_i(t, \theta_2, p) = \theta_1 \sum_{\nu} h(\omega_\nu \cdot t) \cdot f(\bar{\mathcal{F}}_\nu[S_i, \theta_2, p]), \tag{44}$$

$$f(\bar{\mathcal{F}}_\nu[S_i, \theta_2]) = \begin{cases} \int_{a(\nu)+p}^{b(\nu)+p} \int_0^{y_{\max}} \bar{\mathcal{F}}_\nu[S_i, \theta_2](\xi, \gamma) d\xi d\gamma, \nu = 1, \ldots, m \\ \int_0^{x_{\max}} \int_{a(\nu)}^{b(\nu)} \bar{\mathcal{F}}_\nu[S_i, \theta_2](\xi, \gamma) d\xi d\gamma, \nu = m+1, \ldots, m+n \end{cases} \tag{45}$$

where p is the position of the frame in an image. The spatial configuration of the frame is chosen to be identical to that of the templates.

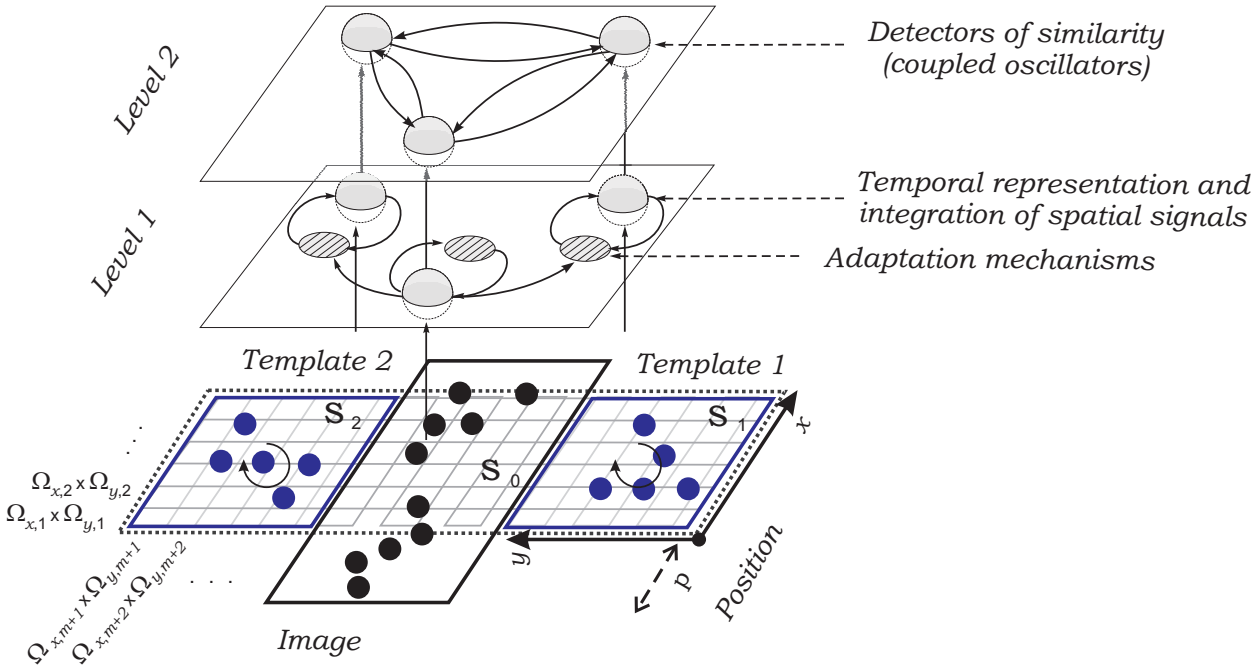

Figure 9: Diagram of the template-matching system detecting multiple objects in an image. The image is viewed through a frame (depicted as a dashed rectangle) generating a temporal representation of the corresponding portion of the image in accordance with (44), (45). This temporal representation is provided to the template subsystems, which search for the values of parameters θ_1 and θ_2 (level 1). The results are passed on to the subsystem detecting coincidence between temporal representations of the templates and the portion of image accessible through the frame

Given that the true positions of the objects in the image are unknown, an extra adaptation mechanism is needed to realize scanning behavior. Table 5 shows an economical way to include such a mechanism into the system. Instead of having an additional compartment within each template subsystem in order to realize the scanning of an image, we propose that the frame of the recognition system moves along the x-coordinate of the image (see also Fig. 9). The equations that govern this motion can be defined as

$$\begin{aligned} p &= p_{\max}\frac{\lambda_{0,1}+1}{2} \\ \dot{\lambda}_{0,1} &= \gamma_0\lambda_{0,2}\min_{i\in\{1,2\}}\{\|\phi_0-\phi_i\|_\varepsilon\} \\ \dot{\lambda}_{0,2} &= -\gamma_0\lambda_{0,1}\min_{i\in\{1,2\}}\{\|\phi_0-\phi_i\|_\varepsilon\}, \end{aligned} \tag{46}$$

where $p_{\max}$ determines the range of scanning. The value of γ_0 is to be chosen small enough and is set to be rationally independent on the value of γ_2 to assure that the conditions of Theorem 1 apply. This ensures that every combination of rotation angles and positions of the templates in the image will be visited in the process of searching.

If we were to detect just one template in the image then adding these new equations (44) – (46) to the previous system would suffice; it would then behave similarly to what is shown in Fig. 8. However, if all patterns need to be recovered, a slight modification of the adaptation algorithms is required.

In systems with weakly attracting sets connected by homoclinic trajectories (see e.g. Fig. 8, the second row) intermittent switching between the attractors can be achieved by arbitrarily small perturbations applied to the solutions. In our case we implement these perturbations by adding a small positive constant δ to the error variables $\|\phi_i(t)-\phi_0(t)\|_\varepsilon$. This is reflected in the adaptation equations of Table 5.

We simulated this simple template-matching system, taking as an input image a combination of two rotated and shifted Garner patterns (Fig. 10, on the right). The system persistently reports the presence of two patterns (Fig. 10, on the left), and successfully estimates their positions and rotation angles. Figure 11 shows the accurately of estimation and demonstrates how much time the system spends in the states corresponding to successful recognition. The latter amounts to about 50 percent of the total time spent; the rest is due to transients. These values can be controlled by parameter $\delta > 0$: the smaller its value δ the more time the system will spend in the state of successful recognition.

An additional observation can be made about this model: in both template subsystems there are domains (e.g., gray areas on the right in the left picture, and the areas on the left in the right picture) that are visited relatively often despite absence of templates in these

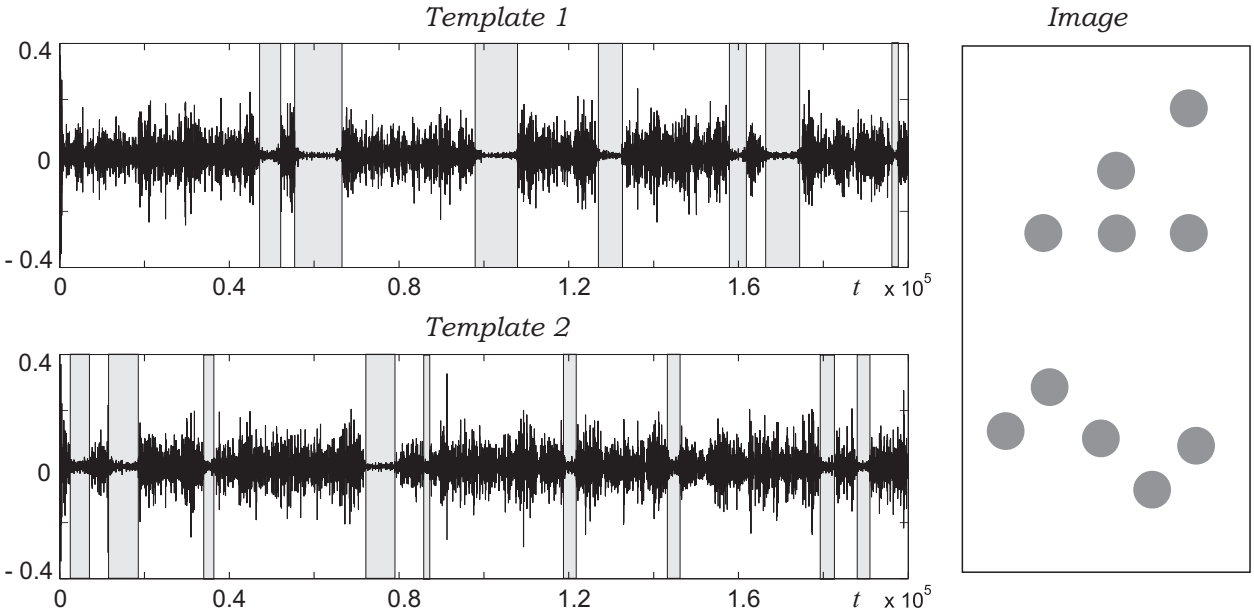

Figure 10: *On the left*: trajectories $x_0(t) - x_1(t)$ (top) and $x_0(t) - x_2(t)$ (bottom) as functions of time. The intervals of time corresponding to synchronized parts of trajectories $x_0(t)$, $x_1(t)$ and $x_2(t)$ are marked by gray rectangles. Synchronization between $x_0(t)$ and $x_1(t)$ corresponds to detection of Template 1 (Garner pattern with no symmetry); and synchronization between $x_0(t)$ and $x_2(t)$ indicates detection of Template 2 (Garner pattern with symmetry). The system switches from one synchronized state to another revealing the complete set of patterns present in the image. *On the right:* input image presented to the system

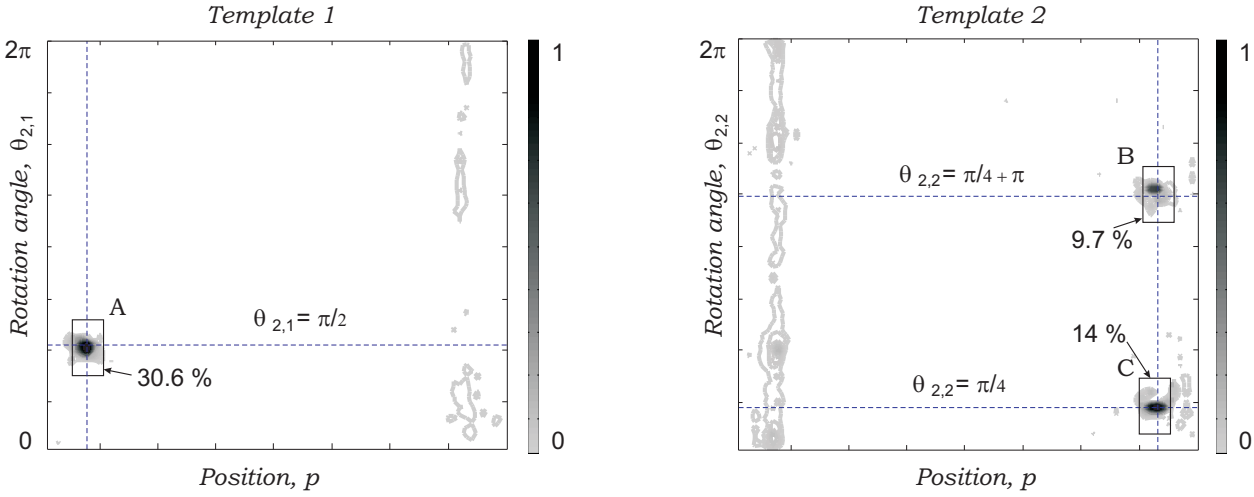

Figure 11: Normalized contour plots of the frequencies with which trajectories $(\hat{\theta}_{2,i}(t), p(t))$ explore the parameter space of the modeled perturbations (rotation and translation). The left panel corresponds to the Garner pattern with no symmetries (Template 1), and the right panel corresponds to the pattern with one symmetry (Template 2). As these pictures demonstrate, the system spends most of time in the small vicinities of true values of θ_2 and p. In the case of Template 2 the most visited set consists of two separated domains corresponding to two values of θ_2 with identical temporal representation due to the symmetry.

Function	Image	Template
Temporal integration	$\dot{\phi}_0 = -\frac{1}{\tau}\phi_0 + k \cdot \theta_1 f(t, \theta_2, p)$	$\dot{\phi}_i = -\frac{1}{\tau}\phi_i + k \cdot \hat{\theta}_{1,i} f(t, \hat{\theta}_{2,i}, 0)$
Adaptation to brightness	No	$\hat{\theta}_{1,i} = (\phi_0 - \phi_i)\gamma_1 + \lambda_{i,1}$ $\dot{\lambda}_{i,1} = \frac{\gamma_1}{\tau}(\phi_0 - \phi_i)$
Adaptation to rotation	No	$\hat{\theta}_{2,i} = (\lambda_{2,i}(t) + 1)\pi$ $\dot{\lambda}_{i,2} = \gamma_2 \lambda_{i,3} \|\phi_0 - \phi_i\|_\varepsilon$ $\dot{\lambda}_{i,3} = -\gamma_2 \lambda_{i,2} \|\phi_0 - \phi_i\|_\varepsilon$
Adaptation position	$p = p_{\max}\frac{\lambda_{0,1}+1}{2}$ $\dot{\lambda}_{0,1} = \gamma_0 \lambda_{0,2} e$ $\dot{\lambda}_{0,2} = -\gamma_0 \lambda_{0,1} e,$ $e = \min_{i \in \{1,2\}} \{\|\phi_0 - \phi_i\|_\varepsilon\} + \delta$	No
Detectors of similarity	$\dot{x}_0 = -ax_0^3 + bx_0^2 + y_0 - z_0 + I + u_0,$ $\dot{y}_0 = c - dx_0^2 - y_0,$ $\dot{z}_0 = \epsilon(s(x_0 + \bar{x}_0) - z_0),$	$\dot{x}_i = -ax_i^3 + bx_i^2 + y_i - z_i + I + u_i + \phi_i(t) - \phi_0(t),$ $\dot{y}_i = c - dx_i^2 - y_i,$ $\dot{z}_i = \epsilon(s(x_i + \bar{x}_0) - z_i),$
Coupling function	$u_0 = \gamma\left(-(N+1)x_0 + \sum_{j \neq 0} x_j\right)$	$u_i = \gamma\left(-(N+1)x_i + \sum_{j \neq i} x_j\right)$
Parameters (additional or having different values than those provided in the previous examples)	Detectors of similarity: $\gamma = 0.4$, $I = 2.2$ Position adaptation subsystem: $\gamma_0 = 0.005/\pi$, $\delta = 0.05$, $p_{\max} = 101$	Rotation adaptation subsystem: $\varepsilon = 0.2$

Table 5: Equations of the system for rotation, position and brightness-invariant template matching in images with multiple objects; N – the total number of templates.

regions. These are phantom states induced by the concurrent presence of several template subsystems. These phantom states occur because the value of p is shared between the template subsystems. If Template 1 is detected then the value of $\min_i \|\phi_i(t) - \phi_0(t)\|$ is

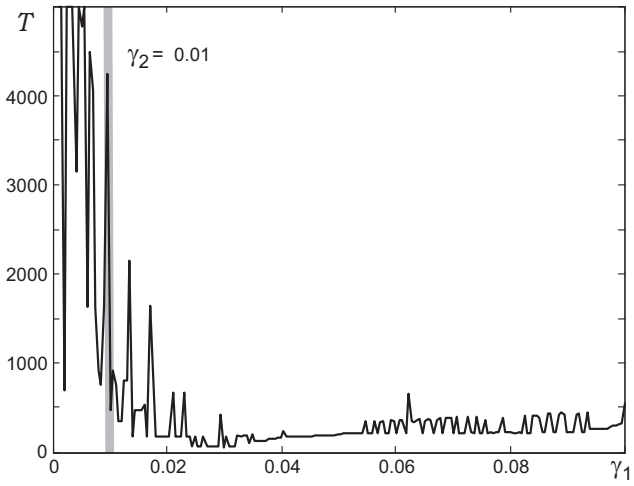

Figure 12: Convergence time T as a function of γ_1. Vertical gray line delimits the domain of γ_1 into two regions: $\gamma_1 \geq \gamma_2$, and $\gamma_1 < \gamma_2$.

small, and position p is not changing much. Because the value of p is shared, the second template subsystem is forced to search for Template 2 in the same position. This property is reflected in the picture on the right.

6.1.3 Effect of differences in time scales

As we mentioned earlier, difference in time scales between adaptation to linearly and nonlinearly parameterized uncertainties is likely to affect recognition performance. In particular, our sufficient conditions suggest that accuracy is smaller when adaptation to linearly parameterized uncertainties is faster than adaptation to nonlinearly parameterized ones. Here we check computationally if this prediction holds for the template matching system considered in Section 6.1.1.

In order to avoid potential influence of image complexity, the Garner patter without symmetries was used. We computed system solutions starting from identical initial conditions but for different values of $\gamma_1 \in [0.005, 0.1]$. In total 200 equally spaced points in this interval were tested. The value of ε, regulating the accuracy of inferring the true value of rotation angle, was set to $\varepsilon = 0.01$. All other parameters were kept identical to the setup described in Section 6.1.1.

For every γ_1 we calculated the amount of time $T(\gamma_1)$ needed for the estimate of rotation angle, $\hat{\theta}_{2,1}$, to converge into a 5-percent neighborhood of its true value, $\pi/4$. This value was chosen as estimate of convergence time. Results of these simulations are summarized in Fig. 12. As we observe, very small values of γ_1, chosen in the interval $[0.005, 0.01]$, result in large convergence times. When the value of γ_1 exceeds a certain threshold, $\gamma_c = 0.02$, convergence

times $T(\gamma_1)$ reduce substantially and remain relatively constant with slight fluctuations for all $\gamma_1 \in [\gamma_c, 0.1]$. Notice that γ_c is two times larger than the value of γ_2 corresponding to the time scale of adaptation to rotation. This supports our initial hypothesis that separate time scales of adaptation may be advantageous for system performance.

6.2 Tracking disturbances in scanning microscopes

We next consider the application of a template-matching system with weakly attracting sets to a problem of realistic complexity. We applied our approach to the problem of tracking morphological changes in dendritic spines based on measurements received from a multiphoton scanning microscope *in vitro*. A distinctive property of laser microscopy is that in order to "see" an object one needs, first, to inject it with a photo-sensitive dye (fluorophore). The particles of the fluorophore emit photons of light under external stimulation, thus illuminating an object from inside the tissue. Typical data from a two-photon microscope are provided in Figure 13[7].

We addressed the problem of how to register fast dynamical changes in spine geometry after application of chemical stimulation. The measurements were performed on slices. Here the need for unstable convergence is motivated by *nonlinearly and non-convexly parameterized models* of uncertainty. Measurements of this kind suffer from effects of photobleaching and diffusion of the dye (see Figure 13), and dependance of the scattering of the emitted light on the *a-priori* unknown position of the object in the slice. On-line estimation and tracking photobleaching (intensity) and changes of the object position (blur) in the slice are therefore necessary.

The measured signal is already a temporal sequence, which fits nicely to our approach. An inherent feature of scanning microscopy is that the object is measured using a sequence of scans along one-dimensional domains (see Figure 13, panel *a*). Hence the objects in this case are one-dimensional mappings, and the domain Ω_x is an interval $\Omega_x = [x_{\min}, x_{\max}]$. For the particular images we set $x_{\min} = 1$ and $x_{\max} = 176$, which corresponds to a scanning line of 176 pixels and 5.95 micro meters. In order to reduce measurement noise we consider the averaged data in the scanning line over n successive subsequent trials.

The measured image, S_0, was chosen to be the averaged data along the scanning line over n successive subsequent trials. The template, S_1, substituted the averaged measurements of the object at the initial time T_1.

Samples of data used to generate S_1 are provided in Figure 14, *a*. These correspond to

[7]The images are provided by S. Grebenyuk, group of neuronal circuit mechanisms, RIKEN BSI

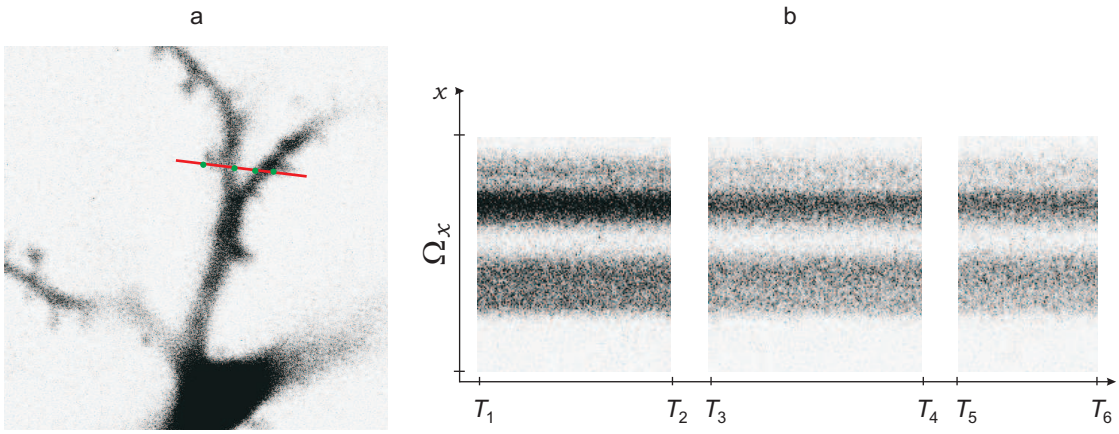

Figure 13: Typical images from the two-photon microscope. Panel a shows a dendrite; the domain of scanning (red line) is in the vicinity of two spines (small protrusions on the dendrite). Size of the domain is 5.95 micron, and speed of scanning, v_s, is 1 pixel per 2 micro seconds. Panel b shows results of scanning as a function of time in the beginning (interval $[T_1, T_2]$), in the middle of experiment (domain $[T_3, T_4]$), and in the end of the experiment (domain $[T_5, T_6]$).

the intensity of the emitted radiation from the object in the red part of the spectrum for the data shown in Figure 13, b, fragment 1. Measured objects, S_0, are the averaged samples of data at the time instants $T_i \neq T_1$ (proportional to T_s). Focal distortions were simulated using conventional filters from Photoshop applied to S_1. These fragments are provided in Figure 14, panels b and c.

The sources of perturbation are the effects of photobleaching (affecting brightness) and deviations in the object position in the slice (affecting scattering and leading to blurred

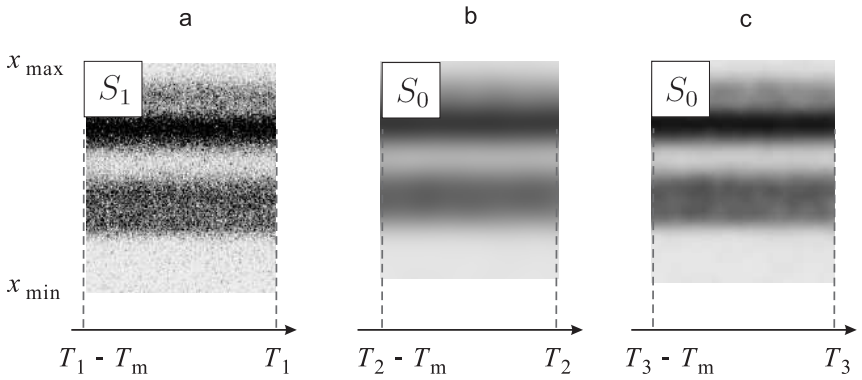

Figure 14: Data which has been used to generate the template, S_1 (panel a), and perturbed measurements S_0 at time instants T_2 and T_3 (panels b and c respectively).

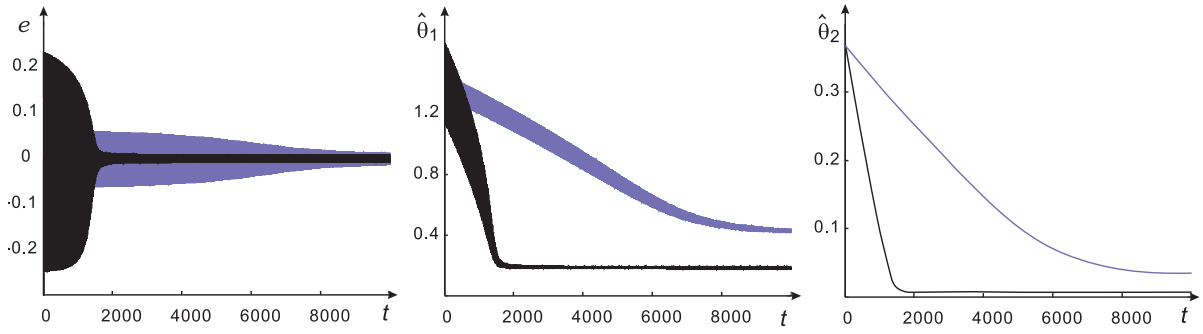

Figure 15: Trajectories $e(t)$, $\hat{\theta}_1(t)$, $\hat{\theta}_2(t)$ as functions of time. Black lines and regions correspond to measurements in Fig. 14, panel *b*. Blue lines and regions correspond to the data in Fig. 14, panel *c*.

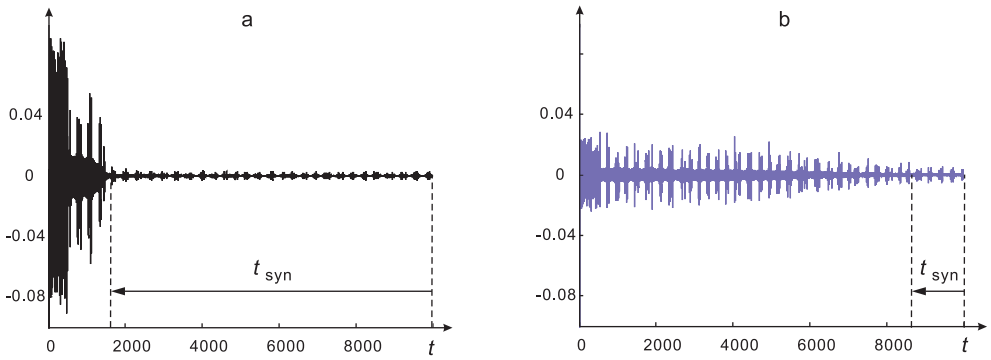

Figure 16: Plots of the synchronization errors $x_0(t) - x_1(t)$ as a function of time. Panel *a* corresponds to the data depicted in Fig. 14, *b*. Panel *b* corresponds to the measurements shown in Fig. 14, *c*.

images). Therefore the following model of uncertainty was used:

$$\theta_1 f_1(x, \theta_2, t) = \theta_1 \int_{\Omega_x} e^{-\theta_2(\xi - x(t))^2} S_1(\xi) d\xi, \tag{47}$$

where $x(t)$, the scanning trajectory in (47), is defined as:

$$x(t) = \begin{cases} x_{\min} + k_s \cdot t & t \le x_{\max} - x_{\min} \\ x(t - (x_{\max} - x_{\min})), & t > x_{\max} - x_{\min} \end{cases}, \; k_s = 1.$$

Figures 15, 16 show the performance of our system (24), (27), (30), (16) in tracking focal/brightness perturbations for two measurements S_0. Figure 15 shows the tracking of unknown modelled perturbations in the images. Figure 16 shows the synchronization errors of the detection subsystem. Symbol t_{syn} denotes "synchronization time" spent in the vicinity of the invariant synchronization manifold. As follows from both figures, the system successfully tracks/reconstructs the estimates of unknown perturbations applied to the object (Fig. 15). Coincidence detectors report synchrony only when the error between

the profiles of the template and object is sufficiently small (Fig. 16). The actual time required for recognition on a standard PC was less than 5 seconds.

7 Conclusion

We provided a principled solution to the problem of invariant template matching on the basis of temporal coding of spatial information. We considered the problem at the levels of mathematical analysis as well as implementation of specific recognition systems. Our analysis showed that a solution to the problem requires us to abandon the traditional notion of stable attractor, in the Lyapunov sense, for defining the target set of a system (van Leeuwen, 1990). As a substitute we proposed the concept of Milnor attracting sets. At the level of implementation we provided systems in which such attractors emerge as a result of external stimulation. These systems are endowed with mathematical rigor in the form of conditions sufficient for ensuring global convergence of trajectories to their target invariant sets. The results provided are normative in the sense that we require a minimal number of additional variables and consider as simple structures as possible.

Even though the proposed system stems from theoretical considerations, it captures qualitatively a wide range of phenomena observed in biological visual perception. These include multiple time scales for different modalities during adaptation (Wolfson & Graham, 2000; Webster et al., 2002; Smith et al., 2006), switching and perceptual multi-stability (Attneave, 1971; Leopold & Logothetis, 1999), the principle of complementarity in perceptual representation (Hatfield & Epstein, 1985), empirical observations in mental rotation (Lachmann & van Leeuwen, 2005) and decision time distributions (Smith & Ratcliff, 2004). The presence of multiple time scales in adaptation could explain the $1/f$ signature of times scales in human behavior (Gilden, 2001). This motivates our belief that present results may contribute to the further understanding of visual perception in biological systems, including humans.

We demonstrated that the problem of invariant recognition can be solved by a simple system of ordinary differential equations with locally Lipschitz right-hand side. This result can be used as an existence proof for solving the problem of adaptive recognition by means of recurrent neural networks with fixed weights. Such systems are being used in various computational tasks (Prokhorov et al., 2002) without any guarantee of a solution. We guarantee that, with such networks, solutions to realistic recognition problems ensuring invariance to rotation, blur, scaling, translation etc. can be obtained.

8 Acknowledgement

The research was supported by a Royal Society International Joint Project grant.

Appendix 1 Optimality of sampled representations

Consider an image $S(x, y)$ and its quantized version S_q obtained from $S(x, y)$ by dividing domain $\Omega_x \times \Omega_y$ into the union of finite number of subsets $\Omega_{x,j} \times \Omega_{y,i}$, $\Omega_x = \cup_j^{N_x} \Omega_{x,j}$, $\Omega_y = \cup_i^{N_y} \Omega_{y,i}$. To each subset $\Omega_{x,j} \times \Omega_{y,i}$ a value is assigned, which can be thought of as the median value of $S(x, y)$ over $\Omega_{x,j} \times \Omega_{y,i}$. We represent S_q as a function of indices i, j: $S_q(i, j)$ and assume that the value of $S_q(i, j)$ is quantized by a set of N_s levels.

Consider a system of sensors which are capable of measuring image $S(x, y)$ instantaneously over the given k-union of subsets $\Omega_{x,j} \times \Omega_{y,i}$. The system's cost can be naturally defined in terms of its total number of sensors. In order to measure the entire image at once the system must have at least $N_x N_y/k$ sensors[8], so in the optimal case its cost C should equal $C(k) = N_x N_y/k$.

We estimate the amount of information contained in this sampled representation of the image. The image is represented by an $N_x N_y/k$-tuple of elements. Each element is assigned a value, say σ_i, from a set of N_s levels with the given probability $p(\sigma_i)$. Hence the entropy of the representation is

$$H(k) = -\sum_i p(\sigma_i) \log \left(\frac{k}{N_x N_y} p(\sigma_i) \right) = \log \left(\frac{N_x N_y}{k} \right) - \sum_i p(\sigma_i) \log p(\sigma_i)$$

The entropy characterizes the informational content of a representation, and function $1/H(k)$ its ambiguity.

Overall losses, $Q(k)$, therefore can be defined as a weighted sum of costs, $C(k)$, and ambiguity, $1/H(k)$:

$$Q(k) = \lambda_1 C(k) + \lambda_2 1/H(k), \ \lambda_1, \lambda_2 \in \mathbb{R}_{>0}, \ k \in [1, N_x N_y]$$

Function $Q(k)$ is unimodal and increasing towards the boundaries of k: $k = 1$, $k = N_x N_y$. This implies that the minimum of $Q(k)$ is achieved for some $k = k^* \in (1, N_x N_y)$. In other words, a representation is optimal only when it is sampled, e.g. induced by a finite, yet neither complete nor elementary, partition of the domain $\Omega_x \times \Omega_y$.

[8]For simplicity we assume that $N_x N_y$ can be expressed as multiples of k.

Appendix 2 Proofs of the theorems

Proof of Theorem 1. We prove the theorem in three steps. First, we show that the solution of the extended system (24), (27), (30) is bounded. Second, we prove that there are constants ρ, b, ε and time instant $t' > 0$ such that the following holds for system solutions:

$$\|\phi_0(t) - \phi_i(t)\|_\varepsilon \leq e^{-\rho(t-t_0)}\|\phi_0(t_0) - \phi_i(t_0)\|_\varepsilon + b\|\theta_2 - \hat{\theta}_{i,2}(\tau)\|_{\infty,[t_0,t]} \quad \forall\, t \geq t_0 > t' \tag{48}$$

Third, using this representation we invoke results from (our paper) and demonstrate that the conclusions of the theorem follow.

1. Boundedness. To prove boundedness of the solutions of the extended system in forward time let us first consider the difference $e_i(t) = \phi_0(t) - \phi_i(t)$. According to (24), dynamics of $e_i(t)$ will be defined as

$$\dot{e}_i = -\frac{1}{\tau}e_i + k\left(\theta_1 f_i(t,\theta_2) - \hat{\theta}_{i,1} f_i(t,\hat{\theta}_{i,2})\right) + \epsilon(t) \tag{49}$$

Noticing that

$$\theta_1 f_i(t,\theta_2) - \hat{\theta}_{i,1} f_i(t,\hat{\theta}_{i,2}) = [\theta_1 f_i(t,\theta_2) - \theta_1 f_i(t,\hat{\theta}_{i,2})] + [\theta_1 f_i(t,\hat{\theta}_{i,2}) - \hat{\theta}_{i,1} f_i(t,\hat{\theta}_{i,2})]$$

and denoting $\delta_1 = \hat{\theta}_{i,1} - \theta_1$, $\delta_2(t,\theta_1,\theta_2,\hat{\theta}_{i,2}) = \theta_1 f_i(t,\theta_2) - \theta_1 f_i(t,\hat{\theta}_{i,2})$ we can rewrite (49) as follows

$$\dot{e}_i = -\frac{1}{\tau}e_i - \delta_1[k f_i(t,\hat{\theta}_{i,2})] + \delta_2(t,\theta_1,\theta_2,\hat{\theta}_{i,2})k + \epsilon(t) \tag{50}$$

Let us now write equations for $\hat{\theta}_{i,1} - \theta_1$ in (26) in differential form. To do so we differentiate variable $\hat{\theta}_{i,1} - \theta_1 = \delta_1$ with respect to time, taking into account equations (49), (50):

$$\dot{\delta}_1 = -\gamma_1\left(\delta_1[k f_i(t,\hat{\theta}_{i,2})] - \delta_2(t,\theta_1,\theta_2,\hat{\theta}_{i,2})k - \epsilon(t)\right) \tag{51}$$

Variable $\epsilon(t)$ in (51) is bounded according to (23). Let us show that $\delta_2(t,\theta_1,\theta_2,\hat{\theta}_{i,2})$ is also bounded. First of all notice that the following positive definite function

$$V_\lambda = 0.5\left(\lambda_2^2 + \lambda_3^2\right)$$

is not growing with time:

$$\dot{V} = \lambda_2\gamma_2\lambda_3\|\phi_0(t) - \phi_i(t)\|_\varepsilon - \lambda_3\gamma_2\lambda_2\|\phi_0(t) - \phi_i(t)\|_\varepsilon = 0$$

Furthermore

$$\begin{aligned}
\lambda_2(t) &= r\cdot\sin\left(\gamma_2\int_{t_0}^{t}\|\phi_0(\tau) - \phi_i(\tau)\|_\varepsilon d\tau + \varphi_0\right)\\
\lambda_3(t) &= r\cdot\cos\left(\gamma_2\int_{t_0}^{t}\|\phi_0(\tau) - \phi_i(\tau)\|_\varepsilon d\tau + \varphi_0\right),\ r,\varphi_0 \in \mathbb{R}
\end{aligned} \tag{52}$$

Choosing initial conditions $\lambda_2^2(t_0) + \lambda_3^2(t_0) = 1$ ensures that $r = 1$. Hence, according to equation (30), variable $\hat{\theta}_{i,2}$ belongs to the interval $[\theta_{2,\min}, \theta_{2,\max}]$.

Consider variable $\delta_2(t, \theta_1, \theta_2, \hat{\theta}_{i,2})$:

$$\delta_2(t, \theta_1, \theta_2, \hat{\theta}_{i,2}) = \theta_1 f_i(t, \theta_2) - \theta_1 f_i(t, \hat{\theta}_{i,2}(t)) = \theta_1 \left(f_i(t, \theta_2) - f_i(t, \hat{\theta}_{i,2}(t)) \right) \tag{53}$$

Taking into account notational agreement (9), and properties (5), (8), we conclude that the following estimate holds

$$|\delta_2(t, \theta_1, \theta_2, \hat{\theta}_{i,2})| \leq \theta_1 |f_i(t, \theta_2) - f_i(t, \hat{\theta}_{i,2}(t)| \leq \theta_{1,\max} D D_2 |\theta_2 - \hat{\theta}_{i,2}(t)| \tag{54}$$

Given that $\hat{\theta}_{i,2}(t) \in [\theta_{2,\min}, \theta_{2,\max}]$ and using (54) we can provide the following estimate for $\delta_2(t, \theta_1, \theta_2, \hat{\theta}_{i,2})$:

$$|\delta_2(t, \theta_1, \theta_2, \hat{\theta}_{i,2})| \leq \theta_{1,\max} D D_2 |\theta_{2,\max} - \theta_{2,\min}| \tag{55}$$

Let us consider equality (51). According to condition 1) of the theorem, term

$$\alpha(t) = k f_i(t, \hat{\theta}_{i,2}(t))$$

is nonnegative and bounded from below:

$$\alpha(t) = k f_i(t, \hat{\theta}_{i,2}(t)) \geq k D_3, \ \forall \ t \geq 0 \tag{56}$$

Taking into account equations (51), (56) we can estimate $|\delta_1(t)|$ as follows:

$$|\delta_1(t)| \leq e^{-\gamma_1 \int_{t_0}^{t} \alpha(\tau) d\tau} |\delta_1(t_0)| + \gamma_1 e^{-\gamma_1 \int_{t_0}^{t} \alpha(\tau) d\tau} \int_{t_0}^{t} e^{\gamma_1 \int_{t_0}^{\tau} \alpha(\tau_1) d\tau_1} |\epsilon(\tau) + \delta_2(\tau) k| d\tau \tag{57}$$

According to (23), (55) we have that for all $t \geq t_0 \geq 0$

$$|\epsilon(t) + \delta_2(t) k| \leq \|\epsilon(\tau) + k \delta_2(\tau)\|_{\infty,[t_0,t]} \leq \Delta + k \theta_{1,\max} D D_2 |\theta_{2,\max} - \theta_{2,\min}| = M_1 \tag{58}$$

Furthermore

$$\int_{t_0}^{t} e^{\gamma_1 \int_{t_0}^{\tau} \alpha(\tau_1) d\tau_1} d\tau = \frac{1}{\gamma_1} \left(\frac{1}{\alpha(t)} e^{\gamma_1 \int_{t_0}^{t} \alpha(\tau) d\tau} - \frac{1}{\alpha(t_0)} \right) \leq \frac{1}{\gamma_1 D_3 k} e^{\gamma_1 \int_{t_0}^{t} \alpha(\tau) d\tau} \tag{59}$$

Taking into account (57), (58), and (59) we can obtain the following estimate:

$$|\delta_1(t)| \leq e^{-\gamma_1 k D_4 (t - t_0)} |\delta_1(t_0)| + \frac{M_1}{D_3 k} \tag{60}$$

Inequality (60) proves that $\delta_1(t)$ is bounded.

In order to complete this step of the proof it is sufficient to show that $e_i(t)$ is bounded. This would automatically imply boundedness of $\phi_i(t)$, thus confirming boundedness of state

of the extended system. To show boundedness of $e_i(t)$ let us write the closed-form solution of (49):

$$e_i(t) = e^{-\frac{(t-t_0)}{\tau}} e_i(t_0) + e^{-\frac{t}{\tau}} \int_{t_0}^{t} e^{\frac{\tau_1}{\tau}} \left(\delta_1(\tau_1)\alpha(\tau_1) + k\delta_2(\tau_1) + \epsilon(\tau_1)\right) d\tau_1 \tag{61}$$

Using (58) and (60) we can derive that

$$|e_i(t)| \leq e^{-\frac{(t-t_0)}{\tau}} |e_i(t_0)| + M_1\tau \left(1 + \frac{D_4}{D_3}\right) + \epsilon_1(t), \tag{62}$$

where $\epsilon_1(t)$ is an exponentially decaying term:

$$|\epsilon_1(t)| \leq e^{-\gamma_1 k D_3 (t-t_0)} \left(\frac{1 - e^{-\left(\frac{1}{\tau} - \gamma_1 k D_3\right)(t-t_0)}}{\frac{1}{\tau} - \gamma_1 k D_3}\right) |\theta_1 - \hat{\theta}_{i,1}(t_0)|. \tag{63}$$

As follows from (52), (60), (62), (63), variables $e_i(t)$, $\hat{\theta}_{i,1}(t)$, $\hat{\theta}_{i,2}(t)$ are bounded. Hence the state of the extended system is bounded in forward time.

2. Transformation. Let us now show that there exists a time instant t' and constants $\rho, c \in \mathbb{R}_{>0}$ such that the dynamics of $e_i(t) = \phi_0(t) - \phi_i(t)$ satisfies inequality (48). In order to do so we first show that term

$$\delta_1(t) k f_i(t, \hat{\theta}_{i,2}(t))$$

in (50) can be estimated as

$$|\delta_1(t) k f_i(t, \hat{\theta}_{i,2}(t))| \leq M_2 |\theta_2 - \hat{\theta}_{i,2}(t)| + \Delta_2 + \epsilon_2(t) \tag{64}$$

where M_2, Δ_2 are positive constants and $\epsilon_2(t)$ is a function of time which converges to zero asymptotically with time.

According to (57) the following holds

$$|\delta_1(t)| \leq e^{-\gamma_1 \int_{t_0}^{t} \alpha(\tau) d\tau} |\delta_1(t_0)| + \gamma_1 e^{-\gamma_1 \int_{t_0}^{t} \alpha(\tau) d\tau} \int_{t_0}^{t} e^{\gamma_1 \int_{t_0}^{\tau} \alpha(\tau_1) d\tau_1} |\epsilon(\tau) + \delta_2(\tau) k| d\tau$$

Taking into account (23), (56) we can conclude that

$$|\delta_1(t)| \leq e^{-\gamma_1 k D_3 (t-t_0)} |\delta_1(t_0)| + \frac{\Delta}{k D_3} + \gamma_1 e^{-\gamma_1 \int_{t_0}^{t} \alpha(\tau) d\tau} \int_{t_0}^{t} e^{\gamma_1 \int_{t_0}^{\tau} \alpha(\tau_1) d\tau_1} |\delta_2(\tau) k| d\tau \tag{65}$$

Substituting (54) into (65) results in

$$\begin{aligned} |\delta_1(t)| \leq & e^{-\gamma_1 k D_3 (t-t_0)} |\delta_1(t_0)| + \frac{\Delta}{k D_3} + \\ & \gamma_1 e^{-\gamma_1 \int_{t_0}^{t} \alpha(\tau) d\tau} \int_{t_0}^{t} e^{\gamma_1 \int_{t_0}^{\tau} \alpha(\tau_1) d\tau_1} |\theta_2 - \hat{\theta}_{i,2}(\tau)| d\tau \cdot (k \theta_{1,\max} D D_2) \end{aligned} \tag{66}$$

Consider the following term in (66):

$$\int_{t_0}^{t} e^{\gamma_1 \int_{t_0}^{\tau} \alpha(\tau_1) d\tau_1} |\theta_2 - \hat{\theta}_{i,2}(\tau)| d\tau \tag{67}$$

Integration of (67) by parts yields

$$\begin{aligned}
&\int_{t_0}^{t} e^{\gamma_1 \int_{t_0}^{\tau} \alpha(\tau_1) d\tau_1} |\theta_2 - \hat{\theta}_{i,2}(\tau)| d\tau = \frac{1}{\gamma_1} \left(\frac{1}{\alpha(t)} e^{\gamma_1 \int_{t_0}^{t} \alpha(\tau) d\tau} |\theta_2 - \hat{\theta}_{i,2}(t)| - \frac{|\theta_2 - \hat{\theta}_{i,2}(t_0)|}{\alpha(t_0)} \right) \\
&- \frac{1}{\gamma_1} \int_{t_0}^{t} \frac{1}{\alpha(\tau)} e^{\gamma_1 \int_{t_0}^{\tau} \alpha(\tau_1) d\tau_1} \left(\frac{d|\theta_2 - \hat{\theta}_{i,2}(\tau)|}{d\tau} \right) d\tau \leq \\
&\frac{1}{\gamma_1 k D_3} e^{\gamma_1 \int_{t_0}^{t} \alpha(\tau) d\tau} |\theta_2 - \hat{\theta}_{i,2}(t)| + \frac{1}{\gamma_1 k D_3} \int_{t_0}^{t} e^{\gamma_1 \int_{t_0}^{\tau} \alpha(\tau_1) d\tau_1} \left| \frac{d|\theta_2 - \hat{\theta}_{i,2}(\tau)|}{d\tau} \right| d\tau
\end{aligned} \tag{68}$$

Given that

$$\hat{\theta}_{2,i} = \theta_{2,\min} + \frac{\theta_{2,\max} - \theta_{2,\min}}{2} (\lambda_2(t) + 1),$$

we can estimate the derivative $d|\theta_2 - \hat{\theta}_{2,i}(t)|/dt$ as follows:

$$\frac{d|\theta_2 - \hat{\theta}_{i,2}(t)|}{dt} \leq \frac{\theta_{2,\max} - \theta_{2,\min}}{2} \cdot \gamma_2 \cdot |\phi_0(t) - \phi_i(t)| \tag{69}$$

Notice that the value of $|\phi_0(t) - \phi_i(t)| = e_i(t)$ in (69) can be estimated according to (62) as

$$|\phi_0(t) - \phi_i(t)| \leq M_1 \tau \left(1 + \frac{D_4}{D_3} \right) + \mu_1(t),$$

where $\mu_1(t) \sim \epsilon_1(t) + e_i(t) e^{-\frac{(t-t_0)}{\tau}}$ is an asymptotically decaying term.

Hence, taking into account (59), (62), (66), (68), and (69) we may conclude that the following inequality holds

$$|\delta_1(t)| \leq \frac{\theta_{1,\max} D D_2}{D_3} |\theta_2 - \hat{\theta}_{i,2}(t)| + \frac{\Delta}{D_3 k} + \frac{\gamma_2}{\gamma_1} \frac{\theta_{1,\max} D D_2}{D_3^2 k} \frac{\theta_{2,\max} - \theta_{2,\min}}{2} M_1 \tau \left(1 + \frac{D_4}{D_3} \right) + \mu(t)$$

where $\mu(t)$ is asymptotically vanishing term. Therefore (64) holds with the following values of M_2 and Δ_2:

$$\begin{aligned}
M_2 &= \frac{k \theta_{1,\max} D D_2 D_4}{D_3} \\
\Delta_2 &= \frac{\gamma_2}{\gamma_1} \left[\frac{\theta_{1,\max} D D_2 D_4}{(D_3)^2} M_1 \tau \left(1 + \frac{D_4}{D_3} \right) \frac{\theta_{2,\max} - \theta_{2,\min}}{2} \right] + \frac{\Delta D_4}{D_3}
\end{aligned} \tag{70}$$

To finalize this step of the proof consider variable $e_i(t)$ for $t \in [t_1, \infty]$, $t_1 \geq t_0$. According to (61), (54) we have that

$$\begin{aligned}
|e_i(t)| \leq\ & e^{-\frac{t-t_1}{\tau}} |e_i(t_1)| + \tau M_2 \|\theta_2 - \hat{\theta}_{i,2}(t)\|_{\infty,[t_1,t]} + \\
& \tau \Delta_2 \left(1 - e^{-\frac{(t-t_1)}{\tau}} \right) + \tau \|\epsilon_2(t)\|_{\infty,[t_1,\infty]} \left(1 - e^{-\frac{(t-t_1)}{\tau}} \right) + \\
& \tau k \theta_{1,\max} D D_2 \|\theta_2 - \hat{\theta}_{i,2}(t)\|_{\infty,[t_1,t]} + \tau \Delta \left(1 - e^{-\frac{(t-t_1)}{\tau}} \right)
\end{aligned} \tag{71}$$

Regrouping terms in (71) yields:

$$|e_i(t)| - \tau\left(\Delta_2 + \Delta + \|\epsilon_2(t)\|_{\infty,[t_1,\infty]}\right) \leq e^{-\frac{t-t_1}{\tau}}\left(|e_i(t_1)| - \tau\left(\Delta_2 + \Delta + \|\epsilon_2(t)\|_{\infty,[t_1,\infty]}\right)\right) + \tau(M_2 + k\theta_{1,\max}DD_2)\|\theta_2 - \hat{\theta}_{i,2}(t)\|_{\infty,[t_1,t]}$$

Denoting

$$\Delta' = \tau\left(\Delta_2 + \Delta + \|\epsilon_2(t)\|_{\infty,[t_1,\infty]}\right) \tag{72}$$

we can obtain

$$\begin{aligned} |e_i(t)| - \Delta' &\leq e^{-\frac{t-t_1}{\tau}}\left(|e_i(t_1)| - \Delta'\right) + \tau(M_2 + k\theta_{1,\max}DD_2)\|\theta_2 - \hat{\theta}_{i,2}(t)\|_{\infty,[t_1,t]} \\ &\leq e^{-\frac{t-t_1}{\tau}}\|e_i(t_1)\|_{\Delta'} + \tau(M_2 + k\theta_{1,\max}DD_2)\|\theta_2 - \hat{\theta}_{i,2}(t)\|_{\infty,[t_1,t]} \end{aligned} \tag{73}$$

Given that

$$\|e_i(t)\|_{\Delta'} = \begin{cases} |e_i(t)| - \Delta', & |e_i(t)| > \Delta' \\ 0, & |e_i(t)| \leq \Delta' \end{cases}$$

and taking into account inequality (73), we can conclude that

$$\|e_i(t)\|_{\Delta'} \leq e^{-\frac{t-t_1}{\tau}}\|e_i(t_1)\|_{\Delta'} + \tau(M_2 + k\theta_{1,\max}DD_2)\|\theta_2 - \hat{\theta}_{i,2}(t)\|_{\infty,[t_1,t]} \tag{74}$$

Because equations (71) – (74) hold for any $t_1 \in (t_0, \infty]$ and that

$$\limsup_{t_1\to\infty} \|\epsilon_2(t)\|_{\infty,[t_1,\infty]} = 0$$

for every

$$\varepsilon > \tau(\Delta + \Delta_2)$$

there exists a time instant $t' \geq t_0$ such that the following inequality is satisfied

$$\|e_i(t)\|_{\varepsilon} \leq e^{-\frac{t-t_1}{\tau}}\|e_i(t_1)\|_{\varepsilon} + \tau(M_2 + k\theta_{1,\max}DD_2)\|\theta_2 - \hat{\theta}_{i,2}(t)\|_{\infty,[t_1,t]} \tag{75}$$

for all $t \geq t_1 \geq t'$. This proves (48) for $\rho = \frac{1}{\tau}$, $b = \tau(M_2 + k\theta_{1,\max}DD_2)$. Hence the second step of the proof is completed.

3. Convergence. In order to prove convergence we employ the following result from (Tyukin et al., 2008):

Lemma 1 (Corollary 3 in (Tyukin et al., 2008)) *Consider the following interconnection of two systems:*

$$\begin{aligned} &\mathcal{S}_a: \ \|\mathbf{x}(t)\|_{\mathcal{A}} \leq \|\mathbf{x}(t_0)\|_{\mathcal{A}} \cdot \beta_t(t - t_0) + c \cdot \|h(\tau)\|_{\infty,[t_0,t]}, \ \mathbf{x}: \mathbb{R}_{\geq 0} \to \mathbb{R}^n \\ &\mathcal{S}_w: \ \int_{t_0}^{t} \underline{\gamma}\,\|\mathbf{x}(\tau)\|_{\mathcal{A}}\, d\tau \leq h(t_0) - h(t) \leq \int_{t_0}^{t} \bar{\gamma}\,\|\mathbf{x}(\tau)\|_{\mathcal{A}}\, d\tau, \ \forall\ t \geq t_0, \ t_0 \in \mathbb{R}_+ \end{aligned} \tag{76}$$

where the systems $\mathcal{S}_a$, $\mathcal{S}_w$ are forward-complete[9]*, function $\beta_t : \mathbb{R}_{\geq 0} \to \mathbb{R}_{\geq 0}$ is strictly monotone and decreases to zero as $t \to \infty$. Let us suppose that the following condition is satisfied*

$$\bar{\gamma} \cdot c \cdot \mathcal{G} < 1, \tag{77}$$

where

$$\mathcal{G} = \beta_t^{-1}\left(\frac{d}{\kappa}\right)\frac{k}{k-1}\left(\beta_t(0)\left(1+\frac{\kappa}{1-d}\right)+1\right)$$

for some $d \in (0,1)$, $\kappa \in (1,\infty)$.

Then there exists a set Ω_γ of initial conditions corresponding to trajectories $\mathbf{x}(t)$, $h(t)$ such that

$$\limsup_{t\to\infty} \|\mathbf{x}(t)\|_{\mathcal{A}} \leq c \cdot h(t_0); \quad h(t) \in [0, h(t_0)] \ \forall\ t \geq t_0$$

In particular, Ω_γ contains the following domain

$$\|\mathbf{x}(t_0)\|_{\mathcal{A}} \leq \frac{1}{\beta_t(0)}\left[\frac{1}{\bar{\gamma}}\left(\beta_t^{-1}\left(\frac{d}{\kappa}\right)\right)^{-1}\frac{k-1}{k} - c\left(\beta_t(0)\left(1+\frac{\kappa}{1-d}\right)+1\right)\right]h(t_0).$$

In order to apply Lemma 1 we need to further transform equations (52), (75) and

$$\hat{\theta}_{i,2}(t) = \theta_{2,\min} + \frac{\theta_{2,\max}-\theta_{2,\min}}{2}(\lambda_2(t)+1) \tag{78}$$

into the form of equation (76). First, we notice that for every $\theta_2 \in [\theta_{2,\min}, \theta_{2,\max}]$ there always exists a real number $\lambda^* \in [-1,1]$ such that

$$\theta_2 = \theta_{2,\min} + \frac{\theta_{2,\max}-\theta_{2,\min}}{2}(\lambda_2^*+1)$$

Hence, denoting

$$c = \tau(M_2 + k\theta_{1,\max}DD_2)\frac{\theta_{2,\max}-\theta_{2,\min}}{2}$$

and using (75) we ascertain that the following holds for solutions of system (24), (27), (30):

$$\|e_i(t)\|_\varepsilon \leq e^{-\frac{t-t_1}{\tau}}\|e_i(t_1)\|_\varepsilon + c\|\lambda_2^* - \lambda_2(t)\|_{\infty,[t_1,t]} \tag{79}$$

for $\varepsilon > \tau(\Delta+\Delta_2)$, and $t \geq t_1 \geq t'$.

Consider the difference $\lambda_2^* - \lambda_2(t)$. According to (52) we have

$$|\lambda_2^* - \lambda_2(t)| \leq |\sigma^* - \int_{t_1}^{t}\gamma_2\|e_i(\tau)\|_\varepsilon - \varphi_0|,\ \lambda_2^* = \sin(\sigma^*) \tag{80}$$

[9]We say that a system is forward-complete iff its state is defined in forward time for all admissible inputs. For the system $\mathcal{S}_a$ the inputs are functions $h(t)$ from $L_\infty[t_0,t]$. For the system $\mathcal{S}_w$ the inputs are locally-bounded in t functions $\mathbf{x}(t)$.

Denoting

$$h(t) = \sigma^* - \int_{t_1}^{t} \gamma_2 \|e_i(\tau)\|_\varepsilon - \varphi_0 \tag{81}$$

and taking into account (79), we therefore obtain the following equations

$$\begin{aligned} \|e_i(t)\|_\varepsilon &\leq e^{-\frac{t-t_1}{\tau}} \|e_i(t_1)\|_\varepsilon + c\|h(t)\|_{\infty,[t_1,t]} \\ h(t_1) - h(t) &= \int_{t_1}^{t} \gamma_2 \|e_i(\tau)\|_\varepsilon d\tau \end{aligned} \tag{82}$$

Equations (82) are a particular case of equations (76) to which Lemma 1 applies. In system (82), however, function $\beta_t(t)$ is defined as $\beta_t(t) = e^{-\frac{t}{\tau}}$. Hence

$$\beta_t^{-1}(t) = -\tau \ln(t)$$

Therefore, according to Lemma 1, satisfying inequality

$$\gamma_2 \cdot c \cdot \tau \ln\left(\frac{\kappa}{d}\right) \frac{k}{k-1} \left(\left(1 + \frac{\kappa}{1-d}\right) + 1\right) < 1 \tag{83}$$

for some $\kappa \in (1, \infty)$, $d \in (0, 1)$ ensures existence of initial conditions $e_i(t_1)$, $h(t_1)$ such that $h(t)$ is bounded. Given that

$$\min_{\kappa \in (1,\infty),, d \in (0,1)} \ln\left(\frac{\kappa}{d}\right) \frac{k}{k-1} \left(\left(1 + \frac{\kappa}{1-d}\right) + 1\right) \approx 15.6886 < 16$$

we can rewrite condition (83) in a more conservative, yet simpler form:

$$\gamma_2 \cdot c \cdot \tau < \frac{1}{16}$$

Taking into account notations (70), (81) we can rewrite this inequality as follows:

$$\gamma_2 < \left(\frac{1}{4\tau}\right)^2 \left[k\theta_{1,\max} D D_2 \left(1 + \frac{D_4}{D_3}\right) \left(\frac{\theta_{2,\max} - \theta_{2,\min}}{2}\right)\right]^{-1}$$

Notice that because the function $\sin(\cdot)$ is periodic, the value of σ^* in (80) and, subsequently the value of $h(t_1)$, can be chosen arbitrarily large. Hence for any finite $e_i(t_1)$ and φ_0 there will always exist σ^* and $h(t_1)$ such that variable $h(t)$ is bounded.

Taking into account that $h(t)$ is monotone and bounded, we can conclude that according to the Bolzano-Weierstrass theorem function $h(t)$ has a limit in $[0, h(t_1)]$:

$$\exists h^* \in [0, h(t_1)] : \lim_{t \to \infty} h(t) = h^*.$$

This in turn implies that

$$\lim_{t \to \infty} \int_{t_1}^{t} \gamma_2 \|e_i(\tau)\|_\varepsilon d\tau = \sigma^* - \varphi_0 - h^* < \infty$$

Therefore

$$\exists\ \theta_2' \in [\theta_{2,\min}, \theta_{2,\max}]:\ \lim_{t\to\infty} \hat{\theta}_{i,2}(t) = \theta_{2,\min} + \frac{\theta_{2,\max} - \theta_{2,\min}}{2}(\sin(\sigma^* - \varphi_0 - h^*) + 1) = \theta_2'$$

Moreover, because $\|e_i(t)\|_\varepsilon$ is uniformly continuous in t, convergence of $\|e_i(t)\|_\varepsilon$ to zero as $t \to \infty$ follows immediately from Barbalat's lemma. *The theorem is proven.*

Proof of Theorem 2. The proof consists of three major steps. First, we show that a single Hindmarsh-Rose oscillator is a semi-passive system with radially unbounded storage function (Pogromsky, 1998). In other words, system:

$$\begin{aligned} \dot{x} &= -ax^3 + bx^2 + y - z + I + u \\ \dot{y} &= c - dx^2 - y \\ \dot{z} &= \varepsilon(s(x + x_0) - z), \quad a, b, c, d, \varepsilon, s > 0 \end{aligned} \tag{84}$$

obeys the following inequality

$$V(x(t), y(t), z(t)) - V(x(0), y(0), z(0)) \leq \int_0^t x(\tau)u(\tau) - H(x(\tau), y(\tau), z(\tau))d\tau. \tag{85}$$

where function $H(\cdot)$ is non-negative outside a ball in $\mathbb{R}^3$, and function V is positive definite and radially unbounded. Second, similar to (Pogromsky, 1998), we show that semi-passivity of (84) implies that solutions of the coupled system (16) are bounded. Third, for an arbitrary pair (i, j) of oscillators we present a nonnegative function such that properties (35), (36) hold for sufficiently large values of γ. Then we use the comparison lemma (Khalil, 2002) to complete the proof.

1) Semi-passivity of the Hindmash-Rose oscillator. Let us consider the following class of functions V:

$$V(x, y, z) = \frac{1}{2}\left(c_1x^2 + c_2y^2 + c_3z^2\right)$$

Then showing existence of a function V from the above class which, in addition satisfies inequality

$$\dot{V} \leq xu - H(x, y, z), \tag{86}$$

where H is non-negative outside some ball in $\mathbb{R}^3$, would imply semi-passivity of (84).

Consider the time-derivative of V:

$$\begin{aligned} \dot{V}(x, y, z) = &-c_1ax^4 - c_2dx^2y - c_2y^2 + c_1xy \\ &- c_3\epsilon z^2 + (c_3\epsilon s - c_1)xz + c_1bx^3 + c_1Ix + c_2cy + c_3\epsilon s x_0 z + c_1xu. \end{aligned} \tag{87}$$

Let us rewrite (87) such that the cross terms xy, xz and x^2y are expressed in terms of the powers of x, y, z and their sums. In order to do this we employ the following three equalities:

$$-c_2y^2 + c_1xy = -c_2\lambda_2y^2 - c_2(1-\lambda_2)\Big(y - \frac{c_1}{2c_2(1-\lambda_2)}x\Big)^2 + \frac{{c_1}^2}{4c_2(1-\lambda_2)}x^2 \tag{88}$$

$$-c_3\epsilon z^2 + (c_3\epsilon s - c_1)xz = -c_3\epsilon\lambda_3z^2 - c_3\epsilon(1-\lambda_3)\Big(z - \frac{c_3\epsilon s - c_1}{2c_3\epsilon(1-\lambda_3)}x\Big)^2 + \frac{(c_3\epsilon s - c_1)^2}{4c_3\epsilon(1-\lambda_3)}x^2 \tag{89}$$

$$-c_1ax^4 - c_2dx^2y = -c_1a\lambda_1x^4 - c_1a(1-\lambda_1)\Big(x^2 + \frac{c_2d}{2c_1a(1-\lambda_1)}y\Big)^2 + \frac{(c_2d)^2}{4c_1a(1-\lambda_1)}y^2 \tag{90}$$

In what follows we will assume that constants λ_1, λ_2 and λ_3 in (88)–(90) are chosen arbitrarily in the interval $(0,1)$: $0 < \lambda_i < 1,\ i = 1,2,3$.

Taking equalities (88)–(90) into account, we can rewrite the time derivative of V (equation (87)) in the following form:

$$\begin{aligned}\dot V(x,y,z) = &-c_1a(1-\lambda_1)\Big(x^2 + \frac{c_2d}{2c_1a(1-\lambda_1)}y\Big)^2 - c_2(1-\lambda_2)\Big(y - \frac{c_1}{2c_2(1-\lambda_2)}x\Big)^2 + \\ &- c_3\epsilon(1-\lambda_3)\Big(z - \frac{c_3\epsilon s - c_1}{2c_3\epsilon(1-\lambda_3)}x\Big)^2 - c_2\Big(\lambda_2 - \frac{c_2d^2}{4c_1a(1-\lambda_1)}\Big)y^2 + c_2cy + \\ &- c_3\epsilon\lambda_3z^2 + c_3\epsilon sx_0z - c_1a\lambda_1x^4 + c_1bx^3 + \Big(\frac{{c_1}^2}{4c_2(1-\lambda_2)} + \frac{(c_3\epsilon s - c_1)^2}{4c_3\epsilon(1-\lambda_3)}\Big)x^2 + c_1Ix + c_1xu\end{aligned} \tag{91}$$

Our goal is to express the right-hand side of (91) in the following form:

$$\dot V \le c_1xu + (M - H_0(x,y,z))\,, \tag{92}$$

where $H_0(x,y,z)$ is a radially unbounded nonnegative function outside a ball in $\mathbb{R}^3$, and M is a constant. For this reason we select constants λ_2, c_2 in (86) as follows:

$$\lambda_2 - \frac{c_2d^2}{4c_1a(1-\lambda_1)} > 0, \quad \text{or} \quad \frac{c_2}{c_1} < \frac{4a\lambda_2(1-\lambda_1)}{d^2}. \tag{93}$$

Noticing that

$$\begin{aligned}&-c_2\Big(\lambda_2 - \frac{c_2d^2}{4c_1a(1-\lambda_1)}\Big)y^2 + c_2cy = \\ &\quad -c_2\big(\lambda_2 - \frac{c_2d^2}{4c_1a(1-\lambda_1)}\big)\Big(y - \frac{2cc_1a(1-\lambda_1)}{4\lambda_2c_1a(1-\lambda_1) - c_2d^2}\Big)^2 + \frac{c_1c_2c^2a(1-\lambda_1)}{4\lambda_2c_1a(1-\lambda_1) - c_2d^2}\end{aligned} \tag{94}$$

$$-c_3\epsilon\lambda_3z^2 + c_3\epsilon sx_0z = -c_3\epsilon\lambda_3\Big(z - \frac{sx_0}{2\lambda_3}\Big)^2 + \frac{c_3\epsilon s^2{x_0}^2}{4\lambda_3}$$

proves representation (92) for any fixed $x = \text{const}$. In order to show that (92) holds with respect to the complete set of variables, e.g. (x, y, z) we use the following sequence of equalities:

$$
\begin{aligned}
-c_1 a\lambda_1 x^4 + c_1 b x^3 + \Big(\frac{{c_1}^2}{4c_2(1-\lambda_2)} + \frac{(c_3\epsilon s - c_1)^2}{4c_3\epsilon(1-\lambda_3)}\Big)x^2 + c_1 I x = (\text{see notations below}) \\
-a_0 x^4 + a_1 x^3 + a_2 x^2 + a_3 x + a_4 = \\
-b_0 x^4 - \big(x - b_1\big)^4 + b_2 x^2 + b_3 x + b_4 = \\
-b_0 x^4 - \big(x - b_1\big)^4 + \big(b_2 + d_0\big)x^2 - d_0\big(x - d_1\big)^2 + d_2 = \\
-b_0\big(x^2 - e_0\big)^2 - \big(x - b_1\big)^4 - d_0\big(x - d_1\big)^2 + e_1
\end{aligned} \tag{95}
$$

with

$$
\begin{aligned}
&a_0 = c_1 a\lambda_1,\ a_1 = c_1 b,\ a_2 = \frac{{c_1}^2}{4c_2(1-\lambda_2)} + \frac{(c_3\epsilon s - c_1)^2}{4c_3\epsilon(1-\lambda_3)} \\
&a_3 = c_1 I,\ a_4 = 0\ b_0 = a_0 - 1,\ b_1 = \tfrac{1}{4}a_1,\ b_2 = a_2 + \tfrac{3}{8}{a_1}^2,\ b_3 = a_3 - \tfrac{1}{16}{a_1}^3,\ b_4 = a_4 + \tfrac{1}{256}{a_1}^4 \\
&d_0 = 1,\ d_1 = \frac{b_3}{2d_0},\ d_2 = b_4 + {d_1}^2 d_0,\ e_0 = \frac{b_2 + d_0}{2b_0},\ e_1 = d_2 + b_0 {e_0}^2
\end{aligned} \tag{96}
$$

Notice that we want the value of b_0 in (95), (96) be positive. Hence the value of

$$a_0 = c_1 a\lambda_1$$

should be greater than 1. This can be ensured by choosing the value of c_1 in (86) to be sufficiently large. As a result of this choice, taking restrictions (93) into account, we conclude that the value of c_2 in (86) must be sufficiently small, e.g. satisfy the following inequality:

$$c_2 < c_1 \frac{4a\lambda_2(1-\lambda_1)}{d^2}.$$

The value for d_0 can be chosen arbitrarily, here $d_0 = 1$.

Time-derivative $\dot{V}$ can now be written as follows

$$
\begin{aligned}
\dot{V}(x,y,z) = &-c_1 a(1-\lambda_1)\Big(x^2 + \frac{c_2 d}{2c_1 a(1-\lambda_1)}y\Big)^2 \\
&- c_3\epsilon(1-\lambda_3)\Big(z - \frac{c_3\epsilon s - c_1}{2c_3\epsilon(1-\lambda_3)}x\Big)^2 \\
&- c_2(1-\lambda_2)\Big(y - \frac{c_1}{2c_2(1-\lambda_2)}x\Big)^2 \\
&- c_3\epsilon\lambda_3\Big(z - \frac{s x_0}{2\lambda_3}\Big)^2 + \frac{c_3\epsilon s^2 {x_0}^2}{4\lambda_3} + \\
&- c_2\big(\lambda_2 - \frac{c_2 d^2}{4c_1 a(1-\lambda_1)}\big)\Big(y - \frac{2cc_1 a(1-\lambda_1)}{4\lambda_2 c_1 a(1-\lambda_1) - c_2 d^2}\Big)^2 + \frac{c_1 c_2 c^2 a(1-\lambda_1)}{4\lambda_2 c_1 a(1-\lambda_1) - c_2 d^2} + \\
&- b_0\big(x^2 - e_0\big)^2 - \big(x - b_1\big)^4 - d_0\big(x - d_1\big)^2 + e_1 + c_1 x u
\end{aligned} \tag{97}
$$

It is straightforward to see that expression (97) is of the form (92), where

$$\begin{aligned}H_0(x,y,z) = {} & c_1a(1-\lambda_1)\Big(x^2+\frac{c_2d}{2c_1a(1-\lambda_1)}y\Big)^2+c_3\epsilon(1-\lambda_3)\Big(z-\frac{c_3\epsilon s-c_1}{2c_3\epsilon(1-\lambda_3)}x\Big)^2\\ & +c_2(1-\lambda_2)\Big(y-\frac{c_1}{2c_2(1-\lambda_2)}x\Big)^2+c_3\epsilon\lambda_3\Big(z-\frac{sx_0}{2\lambda_3}\Big)^2\\ & +c_2\big(\lambda_2-\frac{c_2d^2}{4c_1a(1-\lambda_1)}\big)\Big(y-\frac{2cc_1a(1-\lambda_1)}{4\lambda_2c_1a(1-\lambda_1)-c_2d^2}\Big)^2\\ & +b_0\big(x^2-e_0\big)^2+\big(x-b_1\big)^4+d_0\big(x-d_1\big)^2\end{aligned}$$

$$M=\frac{c_3\epsilon s^2{x_0}^2}{4\lambda_3}+\frac{c_1c_2c^2a(1-\lambda_1)}{4\lambda_2c_1a(1-\lambda_1)-c_2d^2}+e_1$$

Let us denote

$$H_1(x,y,z)=H_0-M$$

and rewrite (92) as

$$\dot V\le c_1xu-H_1(x,y,z)$$

Function $H_1(x,y,z)$ is radially unbounded. Furthermore, it is non-negative outside a ball in $\mathbb{R}^3$. Hence choosing

$$V^*(x,y,z)=\frac{1}{c_1}V(x,y,z)$$

we assure existence of (radially unbounded) positive definite $V^*(x,y,z)$ such that

$$\dot V^*\le xu-\frac{H_1(x,y,z)}{c_1},\tag{98}$$

where $H_1(x,y,z)/c_1$ is radially unbounded and non-negative outside a ball in $\mathbb{R}^3$. Thus, according to (86), semi-passivity of the Hindmarsh-Rose system follows.

2) Boundedness of the solutions. We aim to prove that boundedness of $\phi_i(t)$, $i\in\{0,\dots,n\}$ implies boundedness of the state of the coupled system. Without loss of generality we assume that

$$\|\phi_i(\tau)\|_{\infty,[0,\infty]}\le D_\phi$$

Let us denote

$$V_i=V^*(x_i,y_i,z_i),\quad H_{1,i}=\frac{1}{c_1}H_1(x_i,y_i,z_i).$$

Consider the following function

$$V_\Sigma(\mathbf{x},\mathbf{y},\mathbf{z})=\rho\left(\sum_{i=0}^{n}V_i(x_i,y_i,z_i),C\right).\tag{99}$$

where $\mathbf{x}=\mathrm{col}(x_0,\dots,x_n)$, $\mathbf{y}=\mathrm{col}(y_0,\dots,y_n)$, $\mathbf{z}=\mathrm{col}(z_0,\dots,z_n)$ and

$$\rho(s,C)=\begin{cases}s-C, & s\ge C\\ 0, & s<C\end{cases}$$

Function V_Σ is nonnegative for any $C \in \mathbb{R}$ and, furthermore, is radially unbounded. Hence, its boundedness for some $C \in \mathbb{R}$ implies boundedness of x_i, y_i, z_i, $i \in \{0, \ldots, n\}$.

Let us pick $C \in \mathbb{R}$ such that interior of the domain

$$\Omega_C = \{\mathbf{x}, \mathbf{y}, \mathbf{z} \in \mathbb{R} \mid \sum_{i=0}^{n} V_i(x_i, y_i, z_i) \leq C\}$$

contains the domain

$$\sum_{i=0}^{n} H_{1,i}(x_i, y_i, z_i) - \kappa x_i^2 < M_i, \ M_i \in \mathbb{R}_{>0}, \ \kappa \in \mathbb{R}_{>0}$$

where M_i is an arbitrarily large and κ is an arbitrary small positive constant. In other words the following implication holds:

$$\sum_{i=0}^{n} V_i(x_i, y_i, z_i) \geq C \Rightarrow \sum_{i=0}^{n} H_{1,i}(x_i, y_i, z_i) - \kappa x_i^2 \geq M_i \tag{100}$$

Such C always exists because $H_{1,i}(x_i, y_i, z_i) - \kappa x_i^2$ can be expressed as a sum of a nonnegative quadratic form in x_i, y_i, z_i and non-negative functions of the higher order plus a constant, and $V_i(x_i, y_i, z_i)$ is a positive-definite quadratic form.

Consider time-derivative of function $V_\Sigma(\mathbf{x}, \mathbf{y}, \mathbf{z})$. According to (99), (98) it is zero for all $\mathbf{x}, \mathbf{y}, \mathbf{z} \in \Omega_C$, and satisfies the following inequality otherwise:

$$\dot{V}_\Sigma \leq \sum x_i u_i - \sum_{i=0}^{n} H_{1,i}(x_i, y_i, z_i) = \gamma \mathbf{x}^T \Gamma \mathbf{x} + \sum_{i=0}^{n} x_i \phi_i(t) - \sum_{i=0}^{n} H_{1,i}(x_i, y_i, z_i)$$

Using Gershgorin's circle theorem, we can conclude that

$$\dot{V}_\Sigma \leq \sum_{i=0}^{n} x_i \phi_i(t) - \sum_{i=0}^{n} H_{1,i}(x_i, y_i, z_i)$$

Rewriting

$$x_i \phi_i(t) = -\kappa \left(x_i - \frac{\phi_i(t)}{2\kappa} \right)^2 + \kappa x_i^2 + \frac{1}{4\kappa} \phi_i^2(t), \ \kappa > 0$$

leads to the following inequality

$$\dot{V}_\Sigma \leq \kappa \sum_{i=0}^{n} x_i^2 - \sum_{i=0}^{n} \left(H_{1,i}(x_i, y_i, z_i) - \frac{D_\phi^2}{4\kappa} \right) = - \sum_{i=0}^{n} \left(H_{1,i}(x_i, y_i, z_i) - \frac{D_\phi^2}{4\kappa} - \kappa x_i^2 \right)$$

Hence, choosing the value of C such that $M_i \geq D_\phi^2 / 4\kappa$ in (100) we can ensure that

$$\dot{V}_\Sigma \leq 0$$

This implies that $V_\Sigma(\mathbf{x}(t), \mathbf{y}(t), \mathbf{z}(t))$ is not growing with time. Hence trajectories $x_i(t)$, $y_i(t)$, $z_i(t)$ in the coupled system are bounded.

3) Convergence to a vicinity of the synchronization manifold. Consider the i-th and j-th oscillators in (16), $i, j \in \{0, \dots, n\}$, $i \neq j$. Let us introduce the following function

$$V = 0.5 \left(C_x (x_i - x_j)^2 + C_y (y_i - y_j)^2 + C_z (z_i - z_j)^2 \right), \tag{101}$$

where C_x, $C_y > 0$ are to be defined and $C_z = C_x/(s\epsilon)$.

Its time-derivative can be expressed as follows:

$$\begin{aligned} \dot{V} &= -C_x (x_i - x_j)^2 \left(\frac{a x_i^2}{2} + \frac{a x_j^2}{2} + \frac{a (x_i + x_j)^2}{2} - b(x_i + x_j) + \gamma(n+1) \right) \\ &\quad + C_x (y_i - y_j)(x_i - x_j) - C_y d (x_i - x_j)(x_i + x_j)(y_i - y_j) \\ &\quad - C_y (y_i - y_j)^2 - C_z \epsilon (z_i - z_j)^2 + C_x (x_i - x_j)(\phi_i - \phi_j) \end{aligned} \tag{102}$$

Consider the following term in (102):

$$C_x (y_i - y_j)(x_i - x_j) - C_y d (x_i - x_j)(x_i + x_j)(y_i - y_j) - C_y (y_i - y_j)^2.$$

It can be written as follows:

$$\begin{aligned} &\frac{C_x^2}{4 C_y \Delta_1} (x_i - x_j)^2 - \left(\left(\frac{C_x^2}{4 C_y \Delta_1} \right)^{0.5} (x_i - x_j) - (\Delta_1 C_y)^{0.5} (y_i - y_j) \right)^2 + \\ &+ \frac{C_y d^2}{4 \Delta_2} (x_i - x_j)^2 (x_i + x_j)^2 - C_y \left(\left(\frac{d^2}{4 \Delta_2} \right)^{0.5} (x_i^2 - x_j^2) + \Delta_2^{0.5} (y_i - y_j) \right)^2 \\ &- (1 - \Delta_1 - \Delta_2)(y_i - y_j)^2, \end{aligned} \tag{103}$$

where $\Delta_1, \Delta_2 \in \mathbb{R}_{>0}$ and $\Delta_1 + \Delta_2 \in (0, 1)$. Taking (103) into account we rewrite (102) as:

$$\begin{aligned} \dot{V} &\leq -C_x (x_i - x_j)^2 \left(\frac{a x_i^2}{2} + \frac{a x_j^2}{2} + \frac{a (x_i + x_j)^2}{2} - \frac{C_y d^2}{C_x 4 \Delta_2} (x_i + x_j)^2 \right. \\ &\quad \left. - b(x_i + x_j) + \gamma(n+1) - \frac{C_x}{4 C_y \Delta_1} \right) - C_z \epsilon (z_i - z_{i+1})^2 \\ &\quad - C_y (1 - \Delta_1 - \Delta_2)(y_i - y_j)^2 + C_x (x_i - x_j)(\phi_i - \phi_j) \end{aligned} \tag{104}$$

Let

$$\frac{C_y}{C_x} = \frac{2a\Delta_2}{d^2}.$$

Then

$$\begin{aligned} \dot{V} &\leq -C_x (x_i - x_j)^2 \left(\frac{a}{2} \left(x_i - \frac{b}{a} \right)^2 + \frac{a}{2} \left(x_j - \frac{b}{a} \right)^2 + \gamma(n+1) - \frac{d^2}{8 a \Delta_1 \Delta_2} - \frac{b^2}{a} \right) \\ &\quad - (1 - \Delta_1 - \Delta_2) C_y (y_i - y_j)^2 - C_z \epsilon (z_i - z_{i+1})^2 + C_x (x_i - x_j)(\phi_i - \phi_j). \end{aligned} \tag{105}$$

Hence, choosing

$$\gamma > \frac{1}{(n+1)a}\left(\frac{d^2}{8\Delta_1\Delta_2} + b^2\right).$$

we can ensure that the first term in (105) is non-positive. The minimal value of γ ensuring this property can be calculated by minimizing the value

$$\frac{1}{8\Delta_1\Delta_2}$$

for all Δ_1, $\Delta_2 \in \mathbb{R}_{>0}$: $\Delta_1 + \Delta_2 < 1$. This can be done by letting $\Delta_2 = r - \Delta_1$, $r \in (0,1)$ and differentiating the term $1/(8\Delta_1(r-\Delta_1))$ with respect to Δ_1. This leads to the following solution: $\Delta_1 = r/2$, $\Delta_2 = r/2$. Taking this into account we rewrite (105) as follows

$$\begin{aligned}\dot{V} \;\leq\; & -C_x(x_i - x_j)^2\left(\frac{a}{2}\left(x_i - \frac{b}{a}\right)^2 + \frac{a}{2}\left(x_j - \frac{b}{a}\right)^2 + \gamma(n+1) - \frac{d^2}{2ar} - \frac{b^2}{a}\right) \\ & -(1-r)C_y(y_i - y_j)^2 - C_z\epsilon(z_i - z_{i+1})^2 + C_x(x_i - x_j)(\phi_i - \phi_j). \end{aligned} \tag{106}$$

Let

$$\gamma = \frac{1}{(n+1)a}\left(\frac{d^2}{2} + b^2\right) + \varepsilon_1,\ \varepsilon_1 \in \mathbb{R}_{>0}.$$

Alternatively, we can rewrite this as

$$\gamma = \frac{1}{(n+1)a}\left(\frac{d^2}{2r} + b^2\right) + \varepsilon_2,\ r \in (0,1),\ \varepsilon_2 \in \mathbb{R}_{>0}$$

Hence, according to (106) the following inequality holds:

$$\dot{V} \leq -C_x\varepsilon_2(x_i - x_j)^2 - (1-r)C_y(y_i - y_j)^2 - C_z\epsilon(z_i - z_{i+1})^2 + C_x(x_i - x_j)(\phi_i - \phi_j).$$

Then denoting $\alpha = 2\min\{\varepsilon_2, \varepsilon, (1-r)\}$ we obtain

$$\dot{V} \leq -\alpha V + C_x(x_i - x_j)(\phi_i - \phi_j) \tag{107}$$

Consider the following differential equation

$$\dot{\upsilon} = -\alpha\upsilon + C_x(x_i - x_j)(\phi_i - \phi_j) \tag{108}$$

Its solution can be estimated as follows

$$|\upsilon(t)| \leq e^{-\alpha(t-t_0)}|\upsilon(t_0)| + e^{-\alpha t}\int_{t_0}^{t} e^{\alpha\tau}C_x(x_i(\tau) - x_j(\tau))(\phi_i(\tau) - \phi_j(\tau))d\tau$$

for all $t \geq t_0$. Given that $x_i(t)$, $x_j(t)$ are bounded there exists a constant B such that

$$|\upsilon(t)| \leq e^{-\alpha(t-t_0)}|\upsilon(t_0)| + \frac{C_xB}{\alpha}\|\phi_i(\tau) - \phi_j(\tau)\|_{\infty,[t_0,t]}$$

Then, by applying the comparison lemma (see, for example (Khalil, 2002), page 102), we can conclude that

$$V(t) \leq e^{-\alpha(t-t_0)}V(t_0) + \frac{C_xB}{\alpha}\|\phi_i(\tau) - \phi_j(\tau)\|_{\infty,[t_0,t]}.$$

Hence, conclusion 2) of the theorem follows. *The theorem is proven.*

References

Alonso, J. M., Usrey, W. M., & Reid, R. C. (1996). Precisely correlated firing in cells of the lateral geniculate nucleus. *Nature*, *383*, 815-819.

Amit, D., Gutfreund, H., & Sompolinsky, H. (1985). Spin-glass models of neural networks. *Phys. Rev. A*, *32*, 1007-1018.

Amit, Y. (2002). *2D object detection and recognition: Models, algorithms and networks.* MIT Press.

Amit, Y., Grenader, U., & Piccioni, M. (1991). Structural image restoration through deformable templates. *Journal of the American Statistical Association*, *86*(414), 376–387.

Attneave, F. (1971). Multistability in perception. *Sci. Am.*, *225*(6), 63-71.

Baccus, S. A., & Meister, M. (2002). Fast and slow contrast adaptation in retinal circuitry. *Neuron*, *36*, 909–919.

Banham, M., & Katsaggelos, A. (1997). Digital image restoration. *IEEE Signal Processing Magazine*(3), 24–41.

Blake, A., Curwen, R., & Zisserman, A. (1994). A framework for spatiotemporal control in the tracking of visual contours. *International Journal of Computer Vision*, *11*(2), 127–145.

Bueso, M., Angulo, M., Quian, G., & Alonso, F. (1999). Spatial sampling design based on stochastic complexity. *Journal of Multivariate Analysis*(71), 94–110.

Demontis, G., & Cervetto, L. (2002). Vision: how to catch fast signal with slow detectors. *News Physiol Sci*, *17*, 110–114.

Enroth-Cugell, C., Robson, J. G., Scheweitzer-Tong, D. E., & Watson, A. B. (1983). Spatio-temporal integration in can retinal ganglion cells showing linear spatial summation. *J. Physiol. (Lond.)*, *341*, 279–307.

Fradkov, A. L. (1979). Speed-gradient scheme and its applications in adaptive control. *Automation and Remote Control*, *40*(9), 1333–1342.

Fuchs, A., & Haken, H. (1988). Pattern recognition and associative memory as dynamical prosesses in a synergetic system (i and ii). *Biological Cybernetics*, *60*.

Gabor, D. (1946). Theory of communication. *Journal of the Institution of Electrical Engineering*, 429.

Garner, W. R. (1962). *Uncertainty and structure as psychological concepts.* New York.

Gilden, D. L. (2001). Cognitive emissions of 1/f noise. *Psychological Review*, *108*, 33-56.

Gorban, A. (2004). Singularities of transition processes in dynamical systems: Qualitative theory of critical delays electron. *Electr. J. Diff. Eqns. Monograph 5.* (http://ejde.math.txstate.edu/Monographs/05/)

Gorban, A., Tyukin, I., Steur, E., & Nijmeijer, H. (2008). Positive invariance lemmas for a class of control problems with lyapunov-unstable convergence. *Submitted for publication.*

Guckenheimer, J., & Holmes, P. (2002). *Nonlinear oscillations, dynamical systems and bifurcations of vector fields.* Springer.

Gutig, R., & Sompolinsky, H. (2006). The tempotron: a neuron that learns spike timing-based decisions. *Nature Neuroscience*, *9*(3), 420–428.

Hansel, D., & Sompolinsky, H. (1992). Synchronization and computation in a chaotic neural network. *Physical Review Letters*, *68*, 718–721.

Hatfield, G., & Epstein, W. (1985). The status of the minimum principle in the theoretical analysis of visual perception. *Psychological Bulletin*, *97*(2), 155–186.

Herz, A., Suzler, B., Kuhn, R., & Hemmen, J. van. (1989). Hebbian learning reconsidered: Representation of static and dynamic objects in associative neural nets. *Biological Cybernetics*, *60*, 457–467.

Hindmarsh, J., & Rose, R. (1984). A model of neuronal bursting using 3 coupled 1st order differential-equations. *Proc. R. Soc. Lond., B 221*(1222), 87–102.

Hofer, H., & Williams, D. (2002). The eye's mechanisms for autocalibration. *Optics and Photonics News.*

Hopfield, J. J. (1982). Neural networks and physical systems with emergent collective computational abilities. *PNAS*, *79*, 2554–2558.

Izhikevich, E. M. (2004). Which model to use for cortical spiking neurons? *IEEE Transactions on Neural Networks*, *15*, 1063–1070.

Jain, A. K., Duin, R. P. W., & Mao, J. (2000). Statistical pattern recognition: A review. *IEEE Trans. on Pattern Analysis and Machine Inteligence*, *22*(1), 4–37.

Kaneko, K., & Tsuda, I. (2000). *Complex systems: Chaos and beyond.* Springer.

Kaneko, K., & Tsuda, I. (2003). Chaotic itinerancy. *Chaos*, *13*(3), 926–936.

Khalil, H. (2002). *Nonlinear systems (3d edition).* Prentice Hall.

Lachmann, T., & van Leeuwen, C. (2005). Individual pattern representations are context-independant, but their collective representation is context-dependent. *The Quartery Jorunal of Psychology*, *58*(7), 1265-1294.

Lee, T., & Yuille, A. (2006). Efficient coding of visual scenes by grouping and segmentation: theoretical predictions and biological relevance. In K. Doya, S. Ishii, R. Rao, & A. Pougeti (Eds.), *Bayesian brain, probabilistic approaches to neural coding.* MIT Press.

Leeuwenberg, E., & Buffart, H. (1983). An outline of coding theory: summary of some related experiments. In H. G. Geissler, H. Buffart, & E. Leeuwenberg (Eds.), *Modern issues in perception* (pp. 25–47). Amsterdam, NL: North-Holland.

Leopold, D., & Logothetis, N. (1999). Multistable phenomena: changing views in perception. *Trends in Cognitive Science*, *3*(7), 254-264.

Mather, G. (2006). Foundations of perception. *Hove, MA:Psychology Press Ltd.*

Miller, M., & Younes, L. (2001). Group actions, homeomprphisms, and matching: A general framework. *International Journal of Computer Vision*, *41*(1/2), 61–84.

Milnor, J. (1985). On the concept of attractor. *Commun. Math. Phys.*, *99*, 177-195.

Mon-Williams, M., Tresilian, J., Strang, N., Kochhar, P., & Wann, J. (1998). Improving vision: neural compensation for optical defocus. *Proc. R. Soc. Lond B*, *265*(1), 71–77.

Pogromsky, A. Y. (1998). Passivity based design of synchronizing systems. *Int. J. of Bifurc. and Chaos*, *8*(2), 295–319.

Prokhorov, D. V., Feldkamp, L. A., & Tyukin, I. Y. (2002). Adaptive behavior with fixed weights in recurrent neural networks. In *Proc. of IEEE international joint conference on neural networks* (Vol. 3, pp. 2018–2022). Hawaii, USA.

Rabinovic, M. I., Huerta, R., Varona, P., & Aframovich, V. (2008). Transient cognitive dynamics, metastability, and decision-making. *PLOS Computational Biology*, *4*(5), 1–9.

Ritter, H., & Kohonen, T. (1989). Self-organizing semantic maps. *Biological Cybernetics*, *61*, 241–254.

Rodieck, R. W. (1998). The first steps in seeing. *Sunderland, MA: Sinauer Associates, Inc.*

Sharpe, L., & Stockman, A. (1999). Rod pathways: the importance of seeing nothing. *TINS*, *22*, 497-504.

Shepard, R. (1981). Psychophysical complementarity. In M. Kubovy & J. R. Pomeranz (Eds.), *Perceptual organization* (pp. 279–341). Hillsdale, NJ: Erlbaum.

Smirnakis, S., Berry, M., Warland, D., Biallek, W., & Meister, M. (1997). Adaptation of retinal processing to image contrast and spatial scale. *Nature*, *386*, 69–73.

Smith, M. A., Ghazizadeh, A., & Shadmehr, R. (2006). Interacting adaptive processes with different timescales underline short-term motor learning. *PLOS Biology*, *4*(6), 1035–1043.

Smith, P. L., & Ratcliff, R. (2004). Psychology and neurology of simple decisions. *Trends in Neurosceince*, *27*(3), 161–168.

Tsuda, I., & Fujii, H. (2007). Chaos reality in the brain. *J. of Integrative Neuroscience*, *6*(2), 309–326.

Tyukin, I., Prokhorov, & van Leeuwen, C. (2007). Adaptation and parameter estimation in systems with unstable target dynamics and nonlinear parametrization. *IEEE Trans. on Automatic Control*, *52*(9), 1543–1559.

Tyukin, I., Steur, E., Nijmeijer, H., & van Leeuwen, C. (2008). Non-uniform small-gain theorems for systems with unstable invariant sets. *SIAM Journal on Control and Optimization*, *47*(2), 849-882.

Tyukin, I., Tyukina, T., & van Leeuwen, C. (2007). Invariant template matching in systems with temporal coding. *http : //pdl.brain.riken.jp/projects/template_matching/*.

Tyukin, I., & van Leeuwen, C. (2005). Adaptation and nonlinear parameterization: Nonlinear dynamics prospective. In *Proceedings of the 16-th IFAC world congress.* Prague, Czech Republic.

Ullman, S., Vidal-Naquet, M., & Sali, E. (2002). Visual features of intermediate complexity and their use in classification. *Nature Neuroscience*, *5*(7), 682–687.

van Leeuwen, C. (1990). Perceptual-learning systems as conservative structures: Is economy an attractor. *Psychol. Res.*, *52*, 145–152.

van Leeuwen, C. (2008). Chaos breed autonomy: Connectionists design between bias and baby-sitting. *Cogn. Process*, *9*, 83-92.

Webster, M. A., Georgeson, M. A., & Webster, S. (2002). Neural adjustements to image blur. *Nature Neuroscience*, *5*(9), 839–840.

Wolfson, S., & Graham, N. (2000). Exploring the dynamics of light adaptation: the effects of varying the flickering backgrounds duration in the probed-sinewave paradigm. *Vision Research*, *40*(17), 2277–2289.